New stellar reaction rates for ^{25}Mg(p,γ) ^{26}Al and ^{25}Al(p,γ) ^{26}Si

C. Iliadis,[1,2] L. Buchmann,[1] P. M. Endt,[3] H. Herndl,[4] and M. Wiescher[4]
[1]*TRIUMF, 4004 Wesbrook Mall, Vancouver, British Columbia, Canada V6T 2A3*
[2]*McLennan Physical Laboratories, University of Toronto, Toronto, Ontario, Canada M5S 1A7*
[3]*R.J. Van de Graaff Laboratorium, Rijksuniversiteit Utrecht, P.O. Box 80000, 3508 TA Utrecht, The Netherlands*
[4]*Department of Physics, University of Notre Dame, Notre Dame, Indiana 46556*
(Received 10 July 1995)

Existing experimental proton stripping reaction data on ^{25}Mg leading to threshold states in ^{26}Al are reinvestigated and reanalyzed in a consistent and improved manner. We use unbound state form factors in the DWBA analysis of the measured deuteron angular distributions to deduce absolute rather than relative proton partial widths. For higher-lying resonances these values are compared to widths obtained from (p,γ) work. It is also shown that several of the unique J^π values assigned previously to ^{26}Al states are erroneous. This paper reports on a reanalysis of spins, parities, and isospins for ^{26}Al states located at $E_x<8.00$ MeV. We deduce new stellar rates for the reaction ^{25}Mg(p,γ) ^{26}Al and compare our results with previous values. Furthermore, shell-model calculations for the mass $A=26$ system are performed. Theoretical excitation energies, J^π values, γ-ray transition strengths, spectroscopic factors, and proton partial widths are compared to experimental data and new shell-model assignments of experimental states in ^{26}Al are derived. We estimate Coulomb displacement energies of excited ^{26}Mg and ^{26}Si mirror states and present new analog assignments for $T=1$ triplet states in $A=26$ nuclei. Based on shell-model results and analog state information we present updated stellar rates for the ^{25}Al(p,γ) ^{26}Si reaction.

PACS number(s): 25.40.Lw, 26.60.+f, 27.30.+t, 97.10.Cv

I. INTRODUCTION

Extraterrestial γ-ray emission from the isotope ^{26}Al ($E_\gamma=1.8$ MeV) has been observed by spectrometers on board the HEAO 3 spacecraft [1], the SMM satellite [2], several balloon-borne experiments [3,4], and more recently by the Compton Gamma-Ray Observatory (CGRO) [5]. In fact, ^{26}Al was the first radioactive isotope ever seen in extrasolar γ-ray astronomy. The discovery of ^{26}Al in the interstellar medium is of paramount importance. It clearly demonstrates that nucleosynthetic processes are currently active, since the ^{26}Al half-life ($T_{1/2}=7.2\times10^5$ yr) is short compared to the time scale of galactic chemical evolution ($\approx10^{10}$ yr). From the observed γ-ray intensity it is estimated [6] that the production rate of ^{26}Al in the Galaxy is about $3M_\odot$ per 10^6 yr. Furthermore, the discovery that ^{26}Al has decayed *in situ* in various meteoritic inclusions has lead to the observation of a ^{26}Mg excess consistent with an average abundance ratio [7] of ^{26}Al/^{27}Al$=5\times10^{-5}$ at the time of solidification in the Solar System about 4.6×10^9 yr ago. Both discoveries might provide answers to questions regarding the astrophysical sources of ^{26}Al in the Galaxy and on the circumstances and conditions of the Solar System birth. A variety of stellar sites able to produce ^{26}Al have been suggested (for reviews see [6,8]). The most promising candidates appear to be Wolf-Rayet stars, supernovas of type II, nova outbursts, and asymptotic giant branch (AGB) stars. Very recently, the COMPTEL telescope on board CGRO has detected [9] 1.8 MeV γ rays from the Vela region. This observation might present for the first time a possibility of measuring directly the amount of ^{26}Al from an isolated object and could severely constrain nucleosynthesis models.

In the above-mentioned astrophysical sites the isotope ^{26}Al is mainly produced [8] via proton capture on ^{25}Mg in (hydrostatic or explosive) hydrogen burning or carbon-neon burning at stellar temperatures in excess of about $T=0.035$ GK. The ground state of ^{26}Al β decays to the first excited state in ^{26}Mg, giving rise to a 1.8 MeV γ ray from the electromagnetic deexcitation. The isomeric level ($T_{1/2}=6.3$ s) at $E_x=228$ keV β decays predominantly to the ^{26}Mg ground state and, therefore, is of no relevance to the astrophysical observations mentioned earlier. For temperatures $T<0.4$ GK it has been shown in Ref. [10] that no thermal equilibrium is achieved in the stellar environment between the ^{26}Al ground state and the isomeric state. Consequently, both states have to be treated as separate species in nucleosynthesis calculations performed for this temperature range and the γ-ray branching ratio f_0 for forming the ^{26}Al ground state via ^{25}Mg$+p$ has to be known.

The reaction ^{25}Mg(p,γ) ^{26}Al ($Q_{p\gamma}=6307$ keV) was measured by several authors in the proton bombarding energy range $E_p\geqslant198$ keV (for the most recent results see [11]) and the resulting stellar reaction rates are established for temperatures $T>0.2$ GK. For lower stellar temperatures, however, energetically lower-lying resonances corresponding to states near the proton threshold in the compound nucleus ^{26}Al become the major contributors to the reaction rate. Measurements of the ^{25}Mg(p,γ) ^{26}Al reaction at bombarding energies $E_p<198$ keV are extremely difficult to perform using currently available experimental techniques because of Coulomb barrier penetrability considerations. Therefore, resonance strengths for the threshold states in ^{26}Al were calculated [12,13] using proton partial widths derived from the single-particle transfer reaction ^{25}Mg$(^3$He,$d)$ ^{26}Al. The most recent ^{25}Mg$+p$ reaction rates calculated using experimental information from the (p,γ) and $(^3$He,$d)$ reactions are presented in [11–13].

In high-temperature astrophysical environments, such as nova outbursts, the isotope ^{26}Al is produced via the reaction sequence

$$^{24}\mathrm{Mg}(p,\gamma)^{25}\mathrm{Al}(\beta^{+}\nu)^{25}\mathrm{Mg}(p,\gamma)^{26}\mathrm{Al}^{0},$$

where $^{26}\mathrm{Al}^{0}$ denotes the ground state. However, if the $^{25}\mathrm{Al}(p,\gamma)^{26}$Si reaction can compete with the β decay of ^{25}Al ($T_{1/2}=7.2$ s), the production of $^{26}\mathrm{Al}^{0}$ is bypassed, since the subsequent β decay of ^{26}Si populates predominantly the isomeric state rather than the ^{26}Al ground state. A direct measurement of the $^{25}\mathrm{Al}(p,\gamma)^{26}$Si reaction would require the use of a radioactive ^{25}Al beam, but such an experiment has not been attempted yet. The stellar rates for this reaction were previously calculated [14] using experimental information from the mirror nucleus ^{26}Mg together with systematic nuclear trends, and consequently carry large uncertainties.

It should be noted again that the $^{25}\mathrm{Mg}(p,\gamma)^{26}$Al reaction rates for temperatures $T<0.2$ GK rest on the distorted wave Born approximation (DWBA) analysis of proton stripping data from Champagne *et al.* [12] and Rollefson *et al.* [13]. However, the reaction rates reported by these authors deviate by a factor of 3 at $T=0.1$ GK (see Sec. VI). In view of the importance of the $^{25}\mathrm{Mg}+p$ reaction for the stellar production of ^{26}Al we have reanalyzed available data for the $^{25}\mathrm{Mg}(^{3}\mathrm{He},d)$ reaction leading to ^{26}Al threshold states in a consistent and improved manner. The procedure applied and our results are presented in Sec. II. Although ^{26}Al is presently the best-known nucleus in the sd shell [15–17], it became clear in the course of our reinvestigation that several of the unique spin and parity assignments for ^{26}Al states reported earlier [11,12,18] are either erroneous or unjustified. In Sec. III we present a reanalysis of spins, parities, and isospins for ^{26}Al states located at $E_x<8.00$ MeV. Furthermore, we have performed shell-model calculations for the mass $A=26$ system. These calculations are described in Sec. IV and the theoretical results are compared to experimental energies, J^{π} values, γ-ray transition strengths, and spectroscopic factors in order to achieve an improved understanding of the ^{26}Al level structure. The results of Coulomb displacement energy calculations are presented in Sec. V together with newly proposed analog assignments of $T=1$ states in ^{26}Al, ^{26}Mg, and ^{26}Si. New reaction rates for $^{25}\mathrm{Mg}+p$ are presented in Sec. VI and are compared to previous results. In Sec. VII we calculate updated stellar rates for the $^{25}\mathrm{Al}(p,\gamma)^{26}$Si reaction, which are based on the results presented in Sec. V.

Throughout this work, E_p is the proton bombarding energy and E_R labels the resonance energy. All energies are given in the laboratory system unless stated otherwise.

II. REINVESTIGATION OF ^{25}Mg(^{3}He,d)^{26}Al REACTION DATA

A. DWBA treatment of unbound final states

Deuteron angular distributions from the $^{25}\mathrm{Mg}(^{3}\mathrm{He},d)$ reaction leading to ^{26}Al threshold states have been measured by Betts *et al.* [19], Champagne *et al.* [12], and Rollefson *et al.* [13] at bombarding energies of 18, 20, and 15 MeV, respectively. For bound final states the distorted wave Born approximation (DWBA) analysis of the data is straightforward and well established (see, for example, [20]). The calculation of the DWBA cross section reduces to the determination of the distorted waves and bound-state wave functions. In order to achieve agreement between theory and experimental data, the differential cross section is calculated for shell-model wave functions with various values of the transferred orbital angular momentum ℓ until the shape of the cross section is found to agree. The factor by which theory must be multiplied to achieve agreement in magnitude provides the value of the spectroscopic factor S for the final state. However, the states of interest here are located above the proton threshold in ^{26}Al and, consequently, are unbound. The radial form factors no longer decay exponentially as with bound states, but oscillate with constant amplitudes for large radial distances. The DWBA integrands converge very slowly, causing difficulties in the numerical integration. In order to avoid this problem a technique of contour integration in the complex radius plane has been suggested by Vincent and Fortune [21,22]. If the energy dependence of the cross section can be approximated by a Breit-Wigner formula and if the resonance in question is narrow and symmetric, the single-particle stripping cross section for the three-body breakup $A+a\rightarrow B+b\rightarrow A+p+b$ (only particle b observed) is given by

$$\frac{d\sigma}{d\Omega_b}=\frac{\mu_{Ap}k_{Ap}(E_R)}{\hbar^2}\Gamma_p\frac{d\sigma^F(E_R)}{d\Omega_b}, \tag{1}$$

where μ_{Ap} and k_{Ap} are the reduced mass and wave number for the $A+p$ system, respectively. The fictitious cross section $d\sigma^F(E_R)/d\Omega_b$ has the form of the cross section for stripping to a bound state, but the form factor now describes the scattering resonance. From Eq. (1) it can be seen that the differential cross section is proportional to the partial width Γ_p of B for p emission. The corresponding single-particle spectroscopic factor S can be inferred from Γ_p through the relation

$$\frac{\Gamma_p}{\Gamma_{\mathrm{SP}}}=C^2S, \tag{2}$$

where C^2 denotes the isospin Clebsch-Gordan coefficient ($C^2=1/2$ for both $T=0$ and 1 states in $^{25}\mathrm{Mg}+p$). The single-particle partial width Γ_{SP} can simply be obtained [23] by calculating phase shifts as a function of energy for the elastic scattering of nucleons by the appropriate (form factor) optical-model potential. It should be noted that the partial width Γ_p, rather than the spectroscopic factor S, is actually the quantity of astrophysical interest (see Sec. VI).

In Refs. [12,13] the stripping data for the ^{26}Al threshold states have been analyzed using bound-state form factors, e.g., by choosing an excitation energy just below the proton threshold, since it is argued that the differential cross sections do not change noticeably for small changes in excitation energy. Furthermore, these authors calculate proton partial widths for the threshold states in question relative to a higher-lying resonance of known width, assuming that the corresponding states have similar structure (i.e., same orbital angular momentum transfers and comparable spectroscopic strengths). It is claimed [24] that this procedure produces model-independent proton widths; e.g., their results depend only weakly on the choice of the nuclear radius, since only

TABLE I. Optical-model parameters for the ^{25}Mg(^{3}He,d)^{26}Al reaction. [a]

Channel	V (MeV)	r_0 (fm)	a_0 (fm)	W [d] (MeV)	r_W (fm)	a_W (fm)	V_{SO} (MeV)	r_{SO} (fm)	a_{SO} (fm)	r_c (fm)	β [e] (fm)
^{25}Mg+^{3}He [b]	177.0	1.14	0.72	13.0	1.60	0.77	8.0	1.14	0.72	1.40	0.30
^{25}Mg+^{3}He [c]	161.3	1.087	0.798	17.4	1.776	0.751				1.087	0.30
^{26}Al+d [b]	120.0	1.00	0.90	(25–0.5E_x)	1.50	0.50					
^{25}Mg+p [b]	[f]	1.26	0.60				[g]			1.26	0
^{25}Mg+p [c]	[f]	1.25	0.65				[g]			1.25	0

[a]In the notation of Ref. [67].
[b]Values from Ref. [19].
[c]Values from Ref. [12].
[d]Denotes the volume (surface) imaginary potential for the entrance (exit) channel.
[e]Nonlocality parameters β were adopted from Refs. [66,68]; a finite range parameter of 1.54 fm was taken from Ref. [66].
[f]V was chosen to give the separation energy for each level.
[g]A spin-orbit coupling of 25 times the Thomas term was included.

the ratios of Coulomb penetrabilities and spectroscopic factors enter in the calculation of the partial widths. For example, it can be seen from Table II of Ref. [12] that the proton width of the ^{26}Al state at 6364 keV ($J^\pi;T=3^+;1$ and $S_{\ell=0}=0.15$) has been determined relative to the state at 6680 keV ($J^\pi;T=2^+;0$ and $S_{\ell=0}=0.052$). However, it is not clear why these two states of different spins, isospins, and spectroscopic factors should possess similar structure. Furthermore, one has to rely on the fact that both the J^π value and the proton width of the reference resonance are well known. We also note that for certain threshold states the corresponding resonance strengths resulting from the DWBA analysis of Refs. [12,13] disagree (e.g., for the $E_x=6399$ keV state the values deviate by almost a factor of 3).

We have reanalyzed the stripping data of Refs. [12,13,19] by applying the Vincent-Fortune method using unbound-state form factors (i.e., choosing the correct excitation energies of the unbound states) and deduce absolute rather than relative values for the proton partial widths Γ_p. For the higher-lying resonances proton partial widths from both the (p,γ) work and the (^{3}He,d) data are available. A comparison of the respective values represents therefore a stringent test of how

TABLE II. Spectroscopic factors S and proton partial widths Γ_p (in eV) derived from ^{25}Mg(^{3}He,d)^{26}Al reaction data. [a]

E_x	J^π	ℓ	S [b]	S [c]	S [d]	Γ_p [b]	Γ_p [c]	Γ_p [d]	Γ_p [e]	Γ_p [f]
6343	4^-	1,3		0.0077,0.0092 [g]	0.011,0.015 [g]		$\leqslant 3.23\times10^{-20}$	$\leqslant 4.13\times10^{-20}$	$\leqslant 3.23\times10^{-20}$	
	4^+	2+4		0.0085,0.018 [g]	0.0071+0.015		$\leqslant 7.69\times10^{-22}$	6.00×10^{-22}	6.00×10^{-22}	
6364	3^+	0+2	0.19+0.27	0.10+0.27	0.16+0.24	6.05×10^{-13}	3.38×10^{-13}	5.08×10^{-13}	4.83×10^{-13}	
6399	2^-	1+3	0.011+0.042	0.012+0.010	0.020+0.011	2.14×10^{-10}	2.50×10^{-10}	3.73×10^{-10}	2.79×10^{-10}	
6414	0^+	2			0.030			2.52×10^{-10}	2.52×10^{-10}	
6436	5^+	2,4		0.00076,0.0031 [g]	0.0021,0.0092 [g]		$\leqslant 1.66\times10^{-10}$	$\leqslant 4.33\times10^{-10}$	$\leqslant 1.66\times10^{-10}$	
6496	4^+	2+4	0.034+0.016		0.019+0.048	1.95×10^{-6}		1.08×10^{-6}	1.51×10^{-6}	$(9.9\pm1.3)\times10^{-7}$
	5^+	2+4	0.028+0.013		0.015+0.040	1.60×10^{-6}		8.69×10^{-7}	1.23×10^{-6}	$(8.1\pm1.0)\times10^{-7}$
	4^-	1+3	0.011+0.035		0.024,0.050 [h]	2.29×10^{-5}		$\geqslant 4.51\times10^{-8}$	2.29×10^{-5}	$(9.9\pm1.3)\times10^{-7}$
6551	4^+	2+4	0.073+0.077		0.031+0.13	1.07×10^{-4}		4.61×10^{-5}	7.65×10^{-5}	$(6.8\pm0.8)\times10^{-6}$
	5^-	1,3	0.049,0.11 [h]		0.032,0.077 [h]	$\geqslant 2.88\times10^{-6}$		$\geqslant 1.97\times10^{-6}$	$\geqslant 2.43\times10^{-6}$	$(5.6\pm0.7)\times10^{-6}$
6598	5^+									$(5.6\pm0.7)\times10^{-5}$
6610	3^-	1+3	0.14+0.071		0.13+0.030	8.23×10^{-2}		7.77×10^{-2}	8.00×10^{-2}	$(1.2\pm0.2)\times10^{-1}$
6680	2^+	0+2	0.072+0.046		0.065+0.027	1.34		1.21	1.27	$(9.7\pm1.3)\times10^{-1}$
6724	4^-	1+3	0.085+0.055			1.11			1.11	1.2±0.2

[a]Results include finite-range and nonlocality corrections (see Sec. II B).
[b]From reanalysis of data shown in Ref. [19].
[c]From reanalysis of data shown in Ref. [12].
[d]From reanalysis of data shown in Ref. [13].
[e]Average value.
[f]Experimental partial width deduced from the (p,γ) reaction (from measured $\omega\gamma$ [11,30] and Γ_γ/Γ [12,16]).
[g]Deuteron angular distribution did not allow reliable extraction of different ℓ components; therefore, results are presented for pure transfers ℓ and $\ell+2$.
[h]Angular distribution can be fitted with $\ell=3$ component alone; however, small $\ell=1$ component cannot be excluded; results are presented for pure transfers $\ell=1$ and $\ell=3$.

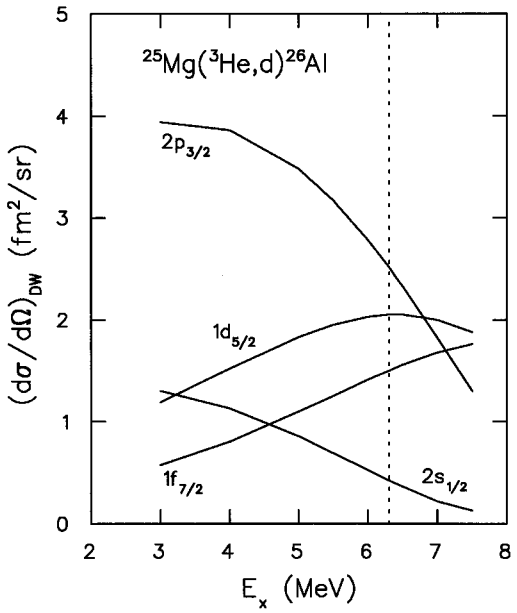

FIG. 1. Calculated DWBA differential cross sections [with $E(^3\mathrm{He})=18$ MeV and $\theta_{\mathrm{c.m.}}=10°$] for different ($n\ell_j$) transfers as a function of excitation energy in the final nucleus. The dashed line indicates the proton threshold.

well this method works. In fact, we will show that the method applied in the present work provides meaningful results and can even be used for the exclusion of certain orbital angular momentum transfers ℓ. We will also show that our absolute proton partial widths are insensitive to the choice of the nuclear radius.

B. Procedure, results, and discussion

The differential cross sections for unbound ^{26}Al states located at $E_x=6343-6724$ keV and displayed in Betts *et al.* [19], Champagne *et al.* [12], and Rollefson *et al.* [13] have been reanalyzed in the present work. The deuteron angular distributions were obtained at three different ^{3}He bombarding energies of 18, 20, and 15 MeV, respectively. It should be noted that Betts *et al.* [19] do not report any spectroscopic factors for unbound ^{26}Al states ($E_x>6.3$ MeV) from the analysis of their measured angular distributions. Furthermore, as already mentioned in Ref. [18] the excitation energies given in their paper are quite poor. Therefore, we have derived more accurate E_x values directly from the deuteron spectrum (their Fig. 1) with the help of a calibration curve based on the (p,γ) energies of strongly excited isolated levels. The DWBA analysis of the data was performed using the program DWUCK4 [25]. The Vincent-Fortune method for the treatment of unbound final states is included in this version of the DWBA code. The numerical values of the optical-model parameters used to generate the distorted waves are listed in Table I. We have used the same values as in the original works [12,13,19] (for a recent discussion of discrete ^{3}He and deuteron optical-model ambiguities for sd-shell nuclei, see Ref. [26]). Finite-range and nonlocality corrections [27] were included in the calculations on the basis of comparing experimental spectroscopic factors to shell-model results (Sec. IV) and the parameters used are also listed in Table I. These corrections, which have a negligible effect on the shapes of the theoretical angular distributions, increase (decrease) the calculated DWBA cross sections (spectroscopic factors) by about 30% compared to the local and zero-range form of the theory.

Since the target spin is not zero, transitions can occur with mixtures of ℓ values differing by two units (e.g., $\ell=0+2$, $1+3$, or $2+4$). A least-squares fitting program was used to compare the experimental angular distributions with DWBA curves for $\ell=0,1,2,3,4$ and for the incoherent sum of ℓ and $\ell+2$. The program searches for the minimum value of the quantity

$$Q^2(\alpha)=\frac{\Sigma_{i,k}[(e_i-\alpha_k t_{ik})/\delta e_i]^2}{i_{\max}-k_{\max}}, \tag{3}$$

where i runs from 1 up to the maximum number of angles at which the cross section was measured ($i_{\max}$), k numbers the ℓ values which are taken into account, ($e_i\pm\delta e_i$) denotes the experimental cross section, and t_{ik} stands for the calculated DWBA cross section at angle i. The constants α_k are proportional to the proton partial widths Γ_p (or spectroscopic factors S). Since the DWBA curves do not exactly describe the experimental angular distributions, Q^2 obviously does not obey a χ^2 distribution. The Q^2 values obtained were nevertheless useful as a criterion for the quality of a fit. The comparison of the proton partial widths derived from the different data sets provides not only information about systematic deviations for measurements at three different ^{3}He bombarding energies, but also on the uncertainties introduced due to the extraction of proton widths for mixed ℓ transfers.

For odd-mass target nuclei, often both $j=\ell-1/2$ and $j=\ell+1/2$ can be added vectorially to the target spin to form the spin of the final state. In the present analysis the $\ell=0$, 1, 2, 3, and 4 curves were calculated assuming $2s_{1/2}$, $2p_{3/2}$, $1d_{5/2}$, $1f_{7/2}$, and $1g_{9/2}$ transfers. For $2p_{1/2}$, $1d_{3/2}$, $1f_{5/2}$, and $1g_{7/2}$ transfers the S values of the present work have to be multiplied by 1.14, 1.27, 1.54, and 2.15, respectively. We have included g transfers in our analysis for two reasons: (i) From the energy spectra of nuclei in the middle of the sd shell it can be seen that states of negative parity ($1\hbar\omega$ excitation) start to occur at $E_x=3-4$ MeV (except for even-even nuclei); therefore, we expect excitations from the sd into the g shell ($2\hbar\omega$ excitation) to occur for $E_x\geqslant 6$ MeV; (ii) the DWBA description of the data improves noticeably for mixed $\ell=2+4$ transfers compared to pure $\ell=2$ transfers. The exclusion of g transfers changes the resulting stellar reaction rates for ^{25}Mg$+p$ (Sec. VI) by a few percent only.

Figure 1 displays DWBA cross sections calculated for $\theta_{\mathrm{c.m.}}=10°$ and $E(^3\mathrm{He})=18$ MeV versus excitation energy E_x of the final ^{26}Al state using the optical-model parameters of Ref. [19]. Any procedure for the DWBA treatment of unbound states does provide meaningful results only if the cross section varies smoothly through the proton threshold (see also Refs. [28,29]). It can be seen that using the Vincent-Fortune method this is indeed the case. Further, it is also clear that neglecting the variation of the cross section with excitation energy (as has been done in Refs. [12,13]) introduces a systematic error even if the Γ_p (or S) values are obtained relative to a reference state (Sec. II A).

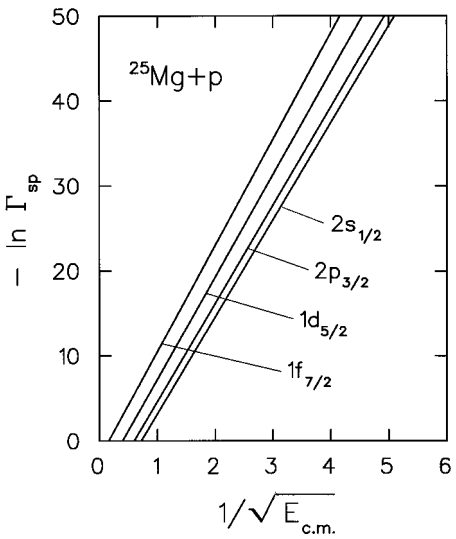

FIG. 2. Proton partial widths versus center-of-mass resonance energies for different ($n\ell_j$) transfers. The widths Γ_{SP} and energies $E_{c.m.}$ are in units of MeV.

Concerning the calculation of single-particle partial widths Γ_{SP} it is a well-known fact [28] that DWUCK4 causes computer overflows for certain choices of excitation (or resonance) energies, especially if the states in question are located just above the threshold. For example, a computation error occurs if one likes to calculate the value for $\Gamma_{SP}(E_x=6364$ keV, $\ell=2)$. Figure 2 shows numerical values of Γ_{SP} versus center-of-mass resonance energies E_R for different ℓ transfers (displayed as $-\ln\Gamma_{SP}$ versus $1/\sqrt{E_{c.m.}}$). It is interesting to note that the resulting curves are well described by linear relationships. All numerical values for Γ_{SP} from the DWUCK4 calculations have been checked by using Fig. 2. If a computer overflow occurred, the correct value of Γ_{SP} was found by interpolation.

Deuteron angular distributions leading to unbound ^{26}Al levels at $E_x=6399$ and 6551 keV are presented in Figs. 3(a) and 3(b), respectively, together with the DWBA fits. It can be seen that similar angular distributions are obtained from appropriate mixtures of either $\ell=0+2$, $1+3$, or $2+4$. This behavior is a direct consequence of the fact that the DWBA curves for pure ℓ transfers become more and more structureless with increasing excitation energy of the final state. These findings do not only apply to the examples shown in Figs. 3(a) and 3(b) but are a common feature of all deuteron angular distributions investigated in the present work. Similar conclusions can be drawn for most ℓ values determined from the (^{3}He,α), (p,d), and (α,t) reactions (for references see [30]) since the measured angular distributions are relatively structureless as well. In this context it is important to note that ℓ values deduced from single-particle stripping and pickup work have been used for the determination of parities

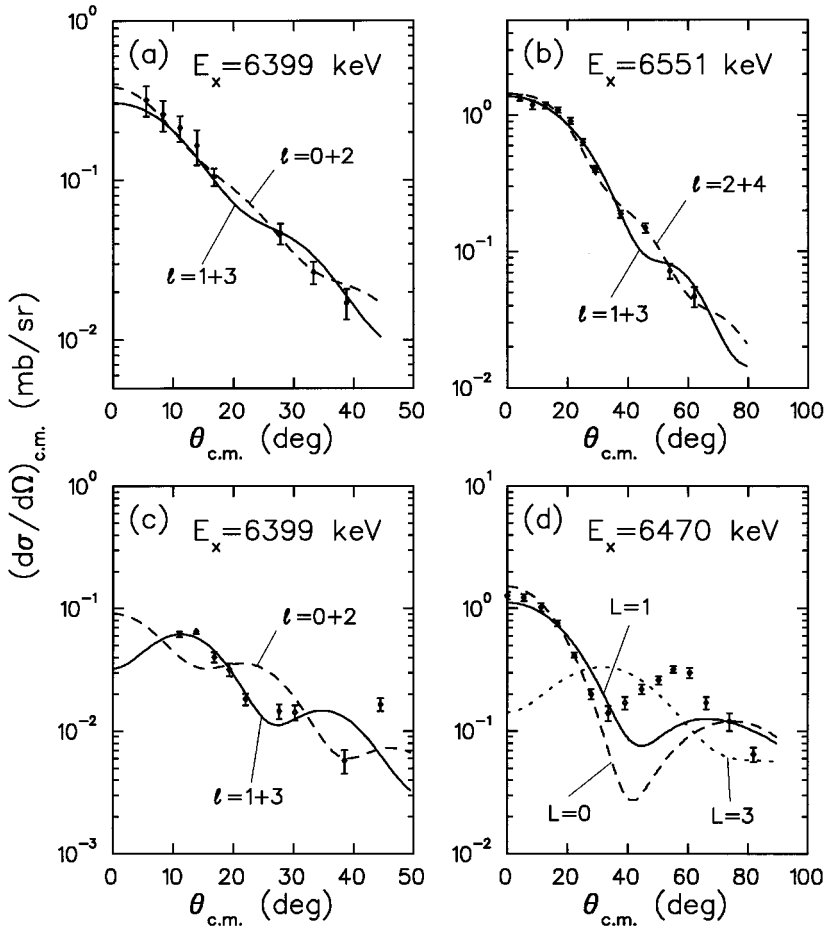

FIG. 3. Experimental angular distributions of the reactions (a) $^{25}Mg(^3He,d)^{26}Al$ [12], (b) $^{25}Mg(^3He,d)^{26}Al$ [13], (c) $^{27}Al(^3He,\alpha)^{26}Al$ [38], and (d) $^{24}Mg(^3He,n)^{26}Si$ [50]. The curves indicate DWBA fits to the data, obtained in the present work for different values of orbital angular momentum transfer.

TABLE III. Strengths[a] and partial widths of low-energy resonances in ^{25}Mg$(p,\gamma)^{26}$Al.

E_x (keV)	E_R (keV)	$J^\pi;T$	Γ_p [b] (eV)	Γ_p [c] (eV)	Γ_p [d] (eV)	$\omega\gamma$ [e] (eV)
6343	38	$4^-;0$	$\leqslant 3.2\times10^{-20}$	$\leqslant 2.8\times10^{-20}$	$(4.2\pm1.0)\times10^{-20}$	$\leqslant 2.4\times10^{-20}$ [f]
		$4^+;0$	6.00×10^{-22}			4.50×10^{-22}
6364	60	$3^+;1$	4.83×10^{-13}	4.5×10^{-13}	$(4.4\pm0.5)\times10^{-13}$	2.82×10^{-13}[f,g]
6399	96	$2^-;0$	2.79×10^{-10}	2.1×10^{-10}	$(5.2\pm1.3)\times10^{-10}$	1.16×10^{-10}[f,g]
6414	112	$0^+;1$	2.52×10^{-10}	$\leqslant 2.4\times10^{-11}$	$(7.5\pm6.0)\times10^{-11}$	2.10×10^{-11}[f,g]
6436	135	$5^+;0$	$\leqslant 1.6\times10^{-10}$			$\leqslant 1.5\times10^{-10}$ [f]

[a]With $\omega\gamma=(2J_R+1)\Gamma_p\Gamma_\gamma/12\Gamma$.
[b]From present work (Table II).
[c]From Ref. [12].
[d]From Ref. [13].
[e]Calculated from average Γ_p values of present work (column 4) using Eq. (5).
[f]Used for the calculation of upper limit for reaction rates.
[g]Used for the calculation of lower limit for reaction rates.

for several ^{26}Al threshold states [30]. In view of the ambiguities involved in the extraction of transferred orbital angular momenta for cases where the transfers can be mixed we generally disregard transfer ℓ values for the determination of parities. In Sec. III we report on a reanalysis of spins, parities, and isospins for ^{26}Al states at $E_x<8.00$ MeV.

The weakest cross sections in the ^{25}Mg(^{3}He,d)^{26}Al reaction have been measured [12,13] for the $E_x=6436$ keV state ($\approx$10–20 μb/sr). The deuteron angular distributions shown are essentially isotropic and, consequently, provide an estimate for a possible compound-nuclear contribution to the observed cross sections. This contribution is negligible for the other threshold states which are much stronger populated (with the possible exception of the astrophysically unimportant $E_x=6414$ keV state; see Sec. VI). On the other hand, a direct reaction component for $E_x=6436$ keV cannot be excluded either. Therefore, we have analyzed the deuteron angular distributions leading to this state using pure ℓ transfers. The resulting proton widths Γ_p represent upper limits. In a few other cases the data could be described by using an $\ell+2$ transfer alone (e.g., for $E_x=6551$ keV assuming $J^\pi=5^-$). However, a (small) ℓ component cannot be excluded. Consequently, the proton partial widths obtained for $\ell+2$ transfer represent lower limits.

Our results of the DWBA analysis for all possible J^π combinations which cannot be excluded on the basis of available experimental information (Sec. III) are presented in Table II. The different columns show orbital angular momenta ℓ, spectroscopic factors S, and proton partial widths Γ_p (using finite range and nonlocality corrections). It can be seen from Table II that the values for S and Γ_p deduced from the different data sets are in reasonable agreement. We also note that our resulting spectroscopic factors agree with the values reported in Ref. [12] (if the latter are corrected for finite range and nonlocality effects), but disagree with the results of Ref. [13] by factors of 2–3 (except for $E_x=6364$ keV). Most of this discrepancy can be explained if it is assumed that these authors list C^2S instead of S in their Table III. The average proton partial widths of the present work are compared in Table III to previous results. Our values are generally in better agreement with Ref. [12] than with the results of Ref. [13].

For states with $E_x>6496$ keV the present average values of total partial widths Γ_p from proton stripping reactions can be compared to results obtained from the (p,γ) work. The latter values have been calculated from the measured resonance strengths $\omega\gamma$ [11,15] and ratios Γ_γ/Γ [12,16] and are listed in the last column of Table II. It can be seen that the agreement is excellent (within a factor of 1.5) except for two combinations of spins and parities: (i) $J^\pi(E_x=6496$ keV$)=4^-$ and (ii) $J^\pi(E_x=6551$ keV$)=4^+$. In these cases the proton widths from stripping and (p,γ) work deviate by factors of 23 and 11, respectively. However, if opposite parities are assumed, the numbers are in agreement (Table II). Both states are relatively strongly populated in the (^{3}He,d) reaction (see the deuteron spectra in Refs. [12,13,19]) and also their angular distributions are equally well described if opposite parities are assumed [Fig. 3(b)]. Since it is unlikely that the transfer widths deviate by such large factors from the (p,γ) widths (see, e.g., Ref. [31]), we have excluded these two J^π combinations. This method of comparing widths from transfer and resonant reactions in order to deduce (or restrict) J^π values has previously been applied in Refs. [32,33]. The new $J^\pi=5^-$ assignment for $E_x=6551$ keV has two consequences. First, this state has been used (on the assumption of $\ell=2$ transfer) by Refs. [12,13] as a reference for the calculation of relative partial widths (Sec. II A). It should be noted, however, that this affects only the $E_x=6414$ keV state which is weakly populated and astrophysically unimportant (Sec. VI). Second, the shell model allows for $E_x<7$ MeV a one-to-one correspondence to experimental states. Therefore, it requires another positive parity state in that excitation range. This aspect is discussed in Sec. IV.

Uncertainties introduced in the calculations of proton widths from transfer data usually include the determination of the absolute experimental cross-section scale, ambiguities in the optical-model potentials, and the extraction of partial widths for mixed ℓ transfers. All these uncertainties are reduced to some extent in the present work since different data sets measured at three ^{3}He bombarding energies have been analyzed consistently. For levels which are strongly populated in the (^{3}He,d) reaction (e.g., $E_x=6364$, 6610, and 6724 keV) we attribute an uncertainty of a factor 1.5 to the aver-

age Γ_p values deduced in the present work. The states at E_x=6343, 6399, 6496, 6551, and 6680 keV are less strongly populated by about an order of magnitude. In these cases the question of multiple-step process contributions to the reaction mechanism arises. For the levels at E_x=6496, 6551, and 6680 keV the proton widths obtained from (^{3}He,d) and (p,γ) reaction data agree within a factor of 1.5, implying a strong direct (single-step) reaction component. However, for the levels at E_x=6343 and 6399 keV, (p,γ) reaction data are not available and the Γ_p values presented in this work (Table II) could be systematically lower by a factor of 2 or even more, depending on the magnitude of multiple-step contributions to the observed cross section.

It is interesting to note that the extracted proton widths are relatively insensitive (within 6%) to variations in both the radius for the unbound form factor and the value of transferred total angular momentum ℓ. For instance, a 10% increase in the radius (e.g., for E_x=6364 keV) increases the single-particle width Γ_{SP} by 20%. Simultaneously, the DWBA cross section also increases by 20%, thus decreasing the extracted spectroscopic factor S by the same amount. Consequently, the product of single-particle width and spectroscopic factor [see Eq. (2)] is insensitive to changes in the radius. Similar arguments apply to the particular choice of the value for $\ell=\ell\pm1/2$.

We conclude this section with a remark concerning the absolute determination of Γ_p values, which has been applied in the present work. It is noted in Ref. [12] that this procedure usually leads to an overestimate of proton widths. To illustrate this point they compare for the states at E_x=6551, 6610, 6680, and 6724 keV absolute Γ_p values from transfer and (p,γ) work which deviate by factors between 1.5 and 37. However, it is clear from the present work that the large discrepancy concerning the E_x=6551 keV state obviously originates from an erroneous J^π assignment. The differences for the other three states are easily explained with the fact that these authors employ simple Γ_p parametrizations using Coulomb penetrabilities instead of performing more realistic optical-model calculations as has been done in the present work.

III. SPINS, PARITIES, AND ISOSPINS FOR ^{26}Al STATES

In this section we present a reanalysis of $J^\pi;T$ assignments for ^{26}Al states located at $E_x\leq$8008 keV. Our results are mainly based on γ-ray transition strengths determined from measured resonance strengths (unbound states) and lifetimes (bound states) using the (p,γ) reaction [15–17]. In Table IV only those levels are listed for which the $J^\pi;T$ assignments differ from the results presented in Ref. [30] or for which the argumentation is different. We also have carefully eliminated ''cyclic reasoning,'' i.e., using a γ-ray transition to limit $J^\pi;T$ of the lower level from that of the upper level *and* vice versa. Furthermore, we have considered recent [34] experimental information obtained from (p,γ) angular distribution measurements.

For the assignments (or restrictions) of J^π and T we have employed the following criteria. (i) The recommended upper limits (RUL's) of Ref. [35] are used. (ii) If necessary, the correspondence with analog states in ^{26}Mg is used for T assignments. (iii) For levels of which lifetimes τ_m or γ-ray widths Γ_γ are unknown the ''dipole+$E2$'' rule [30] rather than RUL's is used. (iv) We use $\ell(p,p_0)$ from Ref. [36]; only for E_x=7773 keV do we also have to adopt their value $J(p,p_0)$=1; only for E_x=7880 keV do we use ℓ_{p_1}=0 from the strength $S(p,p_1)$. (v) For an unresolved doublet the $(\vec{d},\alpha)$ reaction [37] has been used as follows: For $\pi=N$ both components have $\pi=N$; for $\pi=U$ at least one component has $\pi=U$ (N and U denote natural and unnatural parity, respectively). (vi) The ℓ values obtained from single-particle transfer reactions have generally been disregarded except for cases where ℓ=0 (or ℓ=0+2 with a sizable ℓ=0 component), which are recognized unambiguously by the steep rise at very small angles [e.g., see the (^{3}He,d) data [19] for E_x=6280 keV]; we have also used ℓ=1+3 for E_x=6399 keV deduced from (^{3}He,α) reaction data (see below). (vii) The information from the comparison of partial widths Γ_p(^{3}He,d) and $\Gamma_p(p,\gamma)$ has been adopted for E_x=6496 and 6551 keV (Sec. II B). Our new $J^\pi;T$ results are compared in Table IV with the values of Ref. [30]. It can be seen that for several states previously reported unique $J^\pi;T$ assignments have been revised, partially because ℓ values from transfer reactions were disregarded in the present work.

Several states located above the proton threshold are discussed in more detail in the following. For E_x=6343 keV the γ decay yields $J^\pi;T$=(3,4);0, whereas γ feeding (0.42% branching) from the 7222 keV level (with $J^\pi;T=5^+;1$) excludes 3;0. The resulting assignment is $J^\pi;T=4;0$. For the state at E_x=6399 keV the (weak) γ feeding yields $J^\pi;T=(1^+;2);0$. The γ decay of this level is unknown. The measured (^{3}He,α) angular distribution [38] for this state is shown in Fig. 3(c) together with DWBA calculations for mixed transfers ℓ=0+2 and 1+3 (where we have used the same optical-model and form factor parameters as in Ref. [38]). It can be seen that the measured angular distribution clearly cannot be described assuming an even-ℓ transfer. Using ℓ=1+3 leads to the assignment $J^\pi;T=2^-;0$. For E_x=6436 keV the γ decay results in $J^\pi;T=(3-5^+);0$, whereas γ feeding (0.85% branching) from the 7529 keV level (with $J^\pi;T=6^-;0$) excludes J^π=3 and 4^+. The 6436 keV level is fed by the newly discovered [34] 9311 keV state. The measured γ-ray angular distribution of this transition indicates J=5, leading to the final result $J^\pi;T=5^+;0$. Neglecting ℓ(transfer) the $J^\pi;T$ assignment in Ref. [30] for the 6496 keV level should have been $(4,5^+);0$. We disregard the γ-ray branch 6496$\rightarrow$5883 $3^+;0$ reported in Ref. [11], but not observed in Ref. [16]. The use of the recent [34] assignment J=5 from the measured γ-ray angular distribution of the 9060 $4^+;1\rightarrow$6496 transition provides $J^\pi;T=5^+;0$, in agreement with the exclusion of $J^\pi=4^-$ from the comparison of Γ_p(^{3}He,d) and $\Gamma_p(p,\gamma)$ (Sec. II B). For E_x=6551 keV the γ decay leads to $J^\pi;T=(4^+,5^-);0$ if we disregard the transition 6551$\rightarrow$2545 (with 3 2%). The value $J^\pi=4^+$ has been excluded from the comparison of Γ_p(^{3}He,d) and $\Gamma_p(p,\gamma)$ (Sec. II B). Our conclusion is therefore $J^\pi;T=5^-;0$. The very weak γ feeding of E_x=6551 keV is in excellent agreement with $\pi=-$ because of the well-known predominance of $M1$ over $E1$ transitions at the same γ-ray energy (see, e.g., Ref. [16]). For the high-spin levels at E_x=6084, 6892, 7529, and 7548 keV, ℓ=3 has been determined in particle-transfer work (Refs. [39–41]), although the

TABLE IV. Arguments for $J^\pi;T$ assignments to ^{26}Al levels which differ from those in Ref. [30].

E_x (keV)	$J^\pi;T$ from Ref. [30]	$J^\pi;T$ from γ decay [a]	$J^\pi;T$ limitations from resonance feeding (E_x in keV)	Present $J^\pi;T$ assignment
5495	$2^+;0$	$(1^+\text{-}3);0$	$7086 \neq 3;0$, $7425 \neq (1^+,2^-)$	$2^+;0$
5569	$5^+(4);0$	$(3^+\text{-}6^+);0$	$6818 \neq 6^+;0$, $7222 \neq 3^+;0$	$(4,5);0$ [b]
5585	$1^+;0$	$1;0$		$1;0$
5598	$3^-;0$	$(1^+\text{-}3);0$	$6724 \neq (1,2)^+$, $7773 \neq (3,4)^+$	$(2,3)^-;0$ [c]
6084	$5^+;0$	$(4^+,5)$	$6892 \neq 4^+$, $8011\ T=0$	$5^-;0$ [b, d]
6120	$(4,5^+);0$	$(3^+\text{-}6^+)$	$7222\ T=0$, $\neq 3^+$	$(4\text{-}6^+);0$ [e]
6198	$2^+;0$	$(1,2^+)$	$7440\ T=0$	$(1,2^+);0$ [f]
6343	$4^-;0$	$(3,4);0$	$7222 \neq 3$	$4;0$
6399	$2^-;0$	$;0$	$7086 \leqslant 2$, $7464 \geqslant 1^+$	$2^-;0$ [g]
6436	$4^-;0$	$(3\text{-}5^+);0$		$5^+;0$ [h]
6496	$5^+(4^+);0$	$(3\text{-}5^+);0$	$7222 \neq 3$	$5^+;0$ [h, i]
6551	$4^+;0$	$(4^+,5^-);0$		$5^-;0$ [i]
6695 [j]	–	$(4^+\text{-}8^+)$		$7^{(+)};0$ [h]
6802	$1^+(1^-,2^-);1$	$1^+(1^-,2^-);0+1$ [k]		$1^+(1^-,2^-);0+1$
6852	$2^+;1(+0)$	$2^+;0+1$ [k]		$2^+;0+1$
6892	$6^-;0$	$(5^+,6^-);0$		$6^-;0$ [d]
6964	$3^-;1$	$3;1$		$3^-;1$ [l]
7366	$4^+;0$	$(4,5)^+;0$ [m]		$5^+;0$ [h]
7425	$3^+;0$	$(3,4)^+;0$ [n]		$4^+;0$ [h]
7529	$6^-;0$	$(5^+,6^-);0$		$6^-;0$ [d]
7548	$5^-(4^+);0$	$5^-;0$ [d]		$5^-;0$ [d]
7596	$4^+;0$	$(4,5)^+;0$ [o]		$5^+;0$ [h]
7773	$1^-;0$ [p]	$(1^-\text{-}3^+)$		$1^-;0$ [q]
7814	$1^+;0(+1)$	$1^+;0+1$ [r]		$1^+;0+1$
7921	$5^+;0$	$(5,6)^+;0$ [s]		$(5,6)^+;0$
8008	$2^+;0$	$2^+;(0)$ [t]		$2^+;(0)$

[a]Some $T=0$ assignments are based on the argument that for $T=1$ no suitable parent is present in ^{26}Mg.
[b]Previous exclusion of 5^- from feeding is erroneous.
[c]Previous exclusion of 2^- from feeding is erroneous.
[d]See text for a discussion of high-spin $\pi=-$ levels.
[e]Weak feeding from 7874 keV $(3^+;0)$ is disregarded (poor peak shape).
[f]Weak feeding from 7596 keV $(5^+;0)$ and 7953 keV $(4^+;1)$ is disregarded (poor statistics).
[g]With $\pi=-$ from $\ell(^3\text{He},d)=1+3$ (see text).
[h]From angular distribution measurements of γ rays from the $^{25}\text{Mg}(p,\gamma)^{26}$Al reaction (Ref. [34]).
[i]For the exclusion of 4^- for 6496 keV and of 4^+ for 6551 keV from a comparison of the Γ_p values obtained from the (p,γ) and $(^3\text{He},d)$ reactions, see text.
[j]Previously unobserved level.
[k]The increase (as compared to the value in Ref. [30]) of Γ_γ (see Table VII) leads to $T=0+1$.
[l]This is the only state which can be the analog of the 3^- ^{26}Mg 6878 keV level.
[m]The weak decay to the 5495 keV $2^+;0$ level has been disregarded (poor statistics).
[n]The weak p_1 decay used in Ref. [30] to exclude $4^+;0$ does not resonate, but is due to Coulomb excitation (see Fig. 4 of Ref. [15]).
[o]The decay branches to 3751 keV $2^+;0$ (poor statistics) and to 5595 keV $2^+;1$ (formerly assigned to wrong peak) are disregarded.
[p]Erroneously listed as $J;T=1;0$ in Table 23.13 of Ref. [30].
[q]As determined from (p,p_0) in Ref. [36].
[r]Branches to both $T=0$ and $T=1$ levels exceed the RUL($M1_{\text{IS}}$).
[s]At this very weak resonance branches to 3^+ and 4^- levels (all $\leqslant 1.1\%$) have been disregarded.
[t]The decay to the 6028 keV $1^+;1$ level is almost (but not quite) strong enough to prove $T=0$.

DWBA description of the measured differential cross sections for $\ell=3$ is only marginally better than for $\ell=2$. These levels are connected to one another and to eight 4^- and three 5^- states by γ-ray transitions, many of which are surprisingly strong. The corresponding γ-ray branching ratios are presented in Table V. We adopt odd parity for the four levels mentioned above (see Table IV), using again the argument that $M1$ transitions dominate over $E1$ transitions at the same γ-ray energy. More specific information for other ^{26}Al states can be found in Table IV.

TABLE V. Gamma-ray branching ratios (in %) of high-spin odd-parity ^{26}Al levels.[a]

E_{xi} (keV)	$J_i^\pi;T_i$	$J_f^\pi;T_f$: E_{xf}(keV):	$4^-;0$ 5396	$4^-;0$ 5676	$(4^+,5);0$ [b] 6084	$5^-;0$ 6551	$4^-;0$ 6724	$6^-(5^+)$ [b] 6892
6084	$(4^+,5);0$ [b]		0.72 *7*					
6724	$4^-;0$		0.035 *5*	0.034 *4*				
6892	$6^-(5^+);0$ [b]		47 *2*	$\leqslant$0.1	2.3 *1*			
7109	$4^-;0$		0.10 *3*	0.12 *2*	0.62 *3*			
7168	$4^-;0$		0.24 *3*	0.16 *2*	1.23 *4*			
7348	$4^-;1(+0)$		0.20 *2*	0.20 *1*	4.2 *2*	0.17 *2*		
7410	$4^-;1(+0)$		0.29 *4*	0.29 *2*	6.2 *2*	0.32 *1*		
7529	$6^-(5^+);0$ [b]		43 *2*	35 *1*	4.5 *3*			
7548	$5^-(4^+);0$ [b]		2.4 *2*	3.4 *2*	0.78 *12*			0.25 *9*
7825	$4^-;0$		1.0 *2*	0.47 *9*	0.57 *11*			
8011	$5^-;1$		10.6 *4*	16.7 *6*	4.0 *2*		0.18 *6*	4.5 *2*
8067	$5^-;1$		11.5 *4*	18.5 *4*	5.8 *2*			5.1 *2*

[a]Data from Ref. [17]. Resonance branchings below 1% can be obtained from the authors of Ref. [17] on request.

[b]For the parity of these levels, see text.

IV. SHELL-MODEL CALCULATIONS FOR ^{26}Al STATES

The extensive experimental information available [15–17] on the level structure has made ^{26}Al the best-known nucleus in the *sd* shell. A theoretical interpretation of the level scheme using the nuclear shell model has been performed in Ref. [17]. However, neither theoretical spectroscopic factors nor shell-model γ-ray transition strengths connecting many levels at higher excitation energy have been calculated in the previous work. Therefore, we present improved and more extensive calculations and also include our new $J^\pi;T$ assignments (which are based on *experimental* results only) in the comparison between theory and experiment.

Shell-model calculations using the code OXBASH [42] have been performed in the complete $(1d_{5/2}, 2s_{1/2}, 1d_{3/2})$ model space. The single-particle energies employed were $\epsilon(1d_{5/2})=-3948$ keV, $\epsilon(2s_{1/2})=-3164$ keV, and $\epsilon(1d_{3/2})=1647$ keV. For the two-body matrix elements the *W* interaction [43] has been used which includes a mass dependence of the form $A^{-0.3}$. Energy eigenvalues were calculated up to and including $0_3^+;0$, $1_{15}^+;0$, $2_{15}^+;0$, $3_{20}^+;0$, $4_{15}^+;0$, $5_{15}^+;0$, $6_{10}^+;0$, $7_8^+;0$, $8_1^+;0$, $0_6^+;1$, $1_4^+;1$, $2_{10}^+;1$, $3_6^+;1$, $4_{11}^+;1$, $5_5^+;1$, $6_5^+;1$, and $7_1^+;1$. For the calculation of $B(E2)$ values effective charges [44] have been used (1.35*e* for the proton and 0.35*e* for the neutron). Effective *g* factors (which are also mass dependent) for the calculation of $M1$ γ-ray transition strengths were taken from Ref. [45]. Correspondences of theoretical with experimental $\pi=+$ states in ^{26}Al have been made on the basis of comparing excitation energies, $J^\pi;T$ values, γ-ray transition strengths, spectroscopic factors, and proton partial widths. The latter values were calculated from the theoretical spectroscopic factors by using Eq. (2). The experimental energies E_x, widths Γ_γ, and γ-ray branching ratios B_γ were taken from Ref. [30]. Spectroscopic factors for bound and unbound states measured by using proton-transfer reactions have been adopted from Ref. [19] and the present work, respectively. The experimental *S* values were corrected for finite range and nonlocality effects, yielding much better overall agreement with the shell-model calculations. Partial widths Γ_p deduced from proton elastic scattering experiments were taken from Ref. [36]. Configuration and isospin mixing of states has been inferred from the experimental γ-decay branching ratios. In these cases we compare Γ_γ, *S*, and Γ_p values summed over the pair of levels in question. The reader is referred to Ref. [16] for more information concerning this aspect.

Our results are presented in Tables VI and VII for $T=1$ and $T=0$ states, respectively. We do not display the γ decay of single levels in detail (which may involve up to 25 branches), since this kind of comparison would evidently take too much space. However, such a detailed list can be requested from the authors. In the following subsections we present more specific information regarding the nuclear structure of ^{26}Al.

A. $T=1$ $\pi=+$ states of ^{26}Al

The description of the observed $T=1$, $\pi=+$, level structure in ^{26}Al with the shell model is excellent. The lowest 30 $T=1$ shell-model states have experimentally been found with certainty. The $1_3^+;1$, $2_6^+;1$, and $3_4^+;1$ states are isospin-split into two components, respectively, and the $4_6^+;1+4_7^+;1$ states are strongly configuration mixed. We note that all levels with the same $J^\pi;T$ are configuration mixed to some extent, but if the energy separation of neighboring states is very different for experiment and theory, the resulting degree of mixing may also be different. A pleasant surprise is the predominance of $M1_{\rm IV}$ γ decay (as expressed in columns 5 and 10 of Table VI) over other possible (weaker) decay modes. Therefore, the latter decays can be disregarded. On the average the γ-ray branching ratio for $M1_{\rm IV}$ decay amounts to 97% both for experimental and shell-model results (with the isospin-mixed levels omitted). We also note that the introduction of effective *g* factors in the present calculations compared to the use of bare-nucleon *g* factors in Ref. [17] has reduced the average systematic difference between theoretical and experimental well-documented $M1_{\rm IV}$ γ-ray transition strengths from the former

TABLE VI. The ^{26}Al $\pi=+$, $T=1$ states.

Experiment							Shell model [d]						
E_R [a] (keV)	E_x [a] (keV)	$J^\pi;T$ [b]	S [a] $\ell=0+2$	Γ_p [a] (eV)	$M1_{\rm IV}$ decay [c]	τ_m or Γ_γ [a]	E_x (keV)	$J^\pi_n;T$	S $\ell=0+2$	Γ_p (eV)	$M1_{\rm IV}$ decay [c]	τ_m or Γ_γ	[e]
	228	$0^+;1$	,2.4				81	$0^+_1;1$	,2.5				
	3754	$0^+;1$			100	7 *3* fs	3763	$0^+_2;1$	,0.21		100	3.2 fs	A
	5195	$0^+;1$			100	$<$35 fs	5285	$0^+_3;1$	,0.038		99	3.7 fs	A
(112)	6414	$0^+;1$	,0.030 [k]		100		6142	$0^+_4;1$	,0.054		99	0.21 fs	A
	6028	$1^+;1$			89	$<$6 fs	5914	$1^+_1;1$	,0.0035		98	1.3 fs	A
516	6802	$1^+(1^-,2^-);0+1$			80	$>$0.08 eV [h]	6879	$1^+_2;1$	,0.053	0.11	97	2.6 eV	A
1568	7814 [f]	$1^+;0+1$		650	11	1.7 *4* eV	7802	$1^+_3;1$	,0.00045	2.4	100	2.7 eV	B
1637	7880 [f]	$1^+;0+1$			53	8 *2* eV [i]							
	2070	$2^+;1$			97	20 *3* fs	2010	$2^+_1;1$	0.038,0.36		99	10 fs	A
	3160	$2^+;1$	0.54,		99	6 *2* fs	3234	$2^+_2;1$	0.45,0.090		99	2.3 fs	A
	4548	$2^+;1$			100	$<$15 fs	4622	$2^+_3;1$	0.018,0.060		99	1.5 fs	A
	5142	$2^+;1$	0.092,0.023		100	$<$6 fs	5081	$2^+_4;1$	0.062,0.041		100	0.59 fs	A
	5545	$2^+;1$	,0.40		98	22 *19* fs	5485	$2^+_5;1$	0.026,0.45		98	1.6 fs	B
567	6852 [f]	$2^+;0+1$			92	0.76 *8* eV [j]	6728	$2^+_6;1$	0.037,0.058	17.8	99	1.7 eV	A
593	6876 [f]	$2^+;1$			96	0.52 *4* eV [j]							
1043	7308	$2^+;1$			99	1.7 *2* eV [j]	6924	$2^+_7;1$	0.018,0.072	410	100	2.4 eV	A-B
1306	7561	$2^+;1$		3100	97	2.6 *4* eV	7174	$2^+_8;1$	0.024,0.064	1640	95	1.5 eV	B
1744	7982	$2^+;1$		12000	96	3.0 *3* eV	7554	$2^+_9;1$	0.012,0.043	2930	99	3.8 eV	A-B
	4192	$3^+;1$			100	7 *3* fs	4002	$3^+_1;1$	0.22,0.32		99	6.7 fs	A
	4599	$3^+;1$	0.15,0.085		99	7 *3* fs	4592	$3^+_2;1$	0.094,0.061		92	1.6 fs	A
(60)	6364	$3^+;1$	0.15,0.26 [k]		98	32 *16* fs	6349	$3^+_3;1$	0.14,0.32		97	1.0 fs	A
1205	7464 [f]	$3^+;0+1$			75	0.76 *10* eV [j]	7363	$3^+_4;1$	0.011,0.061	625	98	1.8 eV	C
1237	7495 [f]	$3^+;0+1$		80	80	1.2 *2* eV							
1699	7939	$3^+;1$		1700	95	3.6 *4* eV	7683	$3^+_5;1$	0.0073,0.029	1610	97	3.0 eV	A-B
	4705	$4^+;1$	,0.10		100	$<$5 fs	4614	$4^+_1;1$	,0.052		99	1.0 fs	A
	5132	$4^+;1$			94	$<$5 fs	5013	$4^+_2;1$	,0.17		96	3.0 fs	A-B
	5726	$4^+;1$			99	$<$7 fs	5554	$4^+_3;1$	,0.21		98	1.1 fs	A-B
	5924	$4^+;1$			100	$<$17 fs	6090	$4^+_4;1$	,0.031		100	0.56 fs	A
533	6818	$4^+;1$			99	$>$28 meV [h]	6858	$4^+_5;1$	,0.0083	0.025	99	0.66 eV	A
1649	7891 [g]	$4^+;1$		900	99	3.9 *3* eV	7492	$4^+_6;1$	,0.24	1470	99	5.7 eV	A
1714	7953 [g]	$4^+;1$		320	98	4.2 *6* eV	8022	$4^+_7;1$	,0.063	474	98	2.0 eV	
953	7222	$5^+;1$			99	$>$0.70 eV [h]	7119	$5^+_1;1$	,0.017	4.1	97	0.51 eV	A
1375	7628	$5^+;1$		10.0	97	1.4 *1* eV	7546	$5^+_2;1$	,0.0082	18.6	97	1.2 eV	B

[a] From Ref. [30] if not indicated differently; for S values see Sec. II.
[b] From Ref. [30] supplemented with the information in Table IV.
[c] Fraction of γ decay (in %) through $M1_{\rm IV}$ transitions.
[d] The calculations are described in Sec. IV.
[e] Branching agreement, with A, B, and C indicating good, medium, or poor agreement between experimental and shell-model γ-ray branching ratios.
[f] Isospin-mixed doublet.
[g] Configuration-mixed doublet.
[h] The lower limit for Γ_γ is obtained from the (p,γ) yield in Ref. [30].
[i] For a discussion see Sec. IV A.
[j] For these $\ell=0$ resonances we assume $\Gamma_p \gg \Gamma_\gamma$, such that Γ_γ can be obtained from the (p,γ) yield.
[k] From present work (Table II).

factor 1.85 to a few percent. However, the average (logarithmic) difference between the absolute values still amounts to a factor 2.5. The agreement between $\Gamma_\gamma^{\rm expt}$ (taken from Tables 26.13 and 26.18 of Ref. [30]) and $\Gamma_\gamma^{\rm SM}$ (columns 6 and 11) is generally good, with two exceptions.

(i) The difference of a factor 13 for the $E_p=516$ keV $1^+_2;1$ resonance can easily be understood. The $\Gamma_\gamma^{\rm expt}$ value was based on $S(p,\gamma)$ (Table 26.17 of Ref. [30]) combined with the ratio Γ_p/Γ obtained from gamma-ray strength statistics (GRSS) [17]. Using $\Gamma_\gamma^{\rm SM}=2.6$ eV and disregarding GRSS which can only be trusted to a factor 2 we find $\Gamma_p>0.08$ eV from the measured strength $S(p,\gamma)$. This limit is in agreement with the calculated proton width $\Gamma_p^{\rm SM}=0.11$ eV (Table VI).

TABLE VII. The ^{26}Al $\pi=+$, $T=0$ states. [a]

Experiment							Shell model						
E_R (keV)	E_x (keV)	$J^\pi;T$	S $\ell=0+2$	Γ_p (eV)	$M1_{IV}$ decay	τ_m or Γ_γ	E_x (keV)	$J_n^\pi;T$	S $\ell=0+2$	Γ_p (eV)	$M1_{IV}$ decay	τ_m or Γ_γ	
	5462	$0^+(1,2);0$			100 [b]	$<$30 fs	4698	$0_1^+;0$	,0.0010		100 [b]	125 fs	B
	1058	$1^+;0$	,1.43		100	36 *7* fs	818	$1_1^+;0$	,1.40		100	43 fs	A
	1851	$1^+;0$	,0.25		99	46 *5* fs	1737	$1_2^+;0$	,0.23		99	34 fs	A
	2072	$1^+;0$			89	530 *100* fs	2004	$1_3^+;0$	,0.077		99	260 fs	A
	2740	$1^+;0$			99	43 *5* fs	2899	$1_4^+;0$	,0.044		96	119 fs	A
	3724	$1^+;0$			99	6 *2* fs	3685	$1_5^+;0$	,0.00006		99	8.6 fs	A-B
	5010	$1^+;0$			100	$<$9 fs	4938	$1_6^+;0$	,0.029		92	6.6 fs	A
	5585 [c]	1;0			96	$<$8 fs [d]	5154	$1_7^+;0$	,0.14		98	2.2 fs	A
	5671 [c]	$1^+;0$			83	$<$40 fs [d]	5668	$1_8^+;0$	,0.049		96	1.6 fs	
	6270	$1^+;0$			76	$<$13 fs	5944	$1_9^+;0$	,0.11		93	5.1 fs	A-B
591	6874 [c]	$1^+;0$			92	$>$0.05 eV [d]	6658	$1_{10}^+;0$	,0.17	1.2	93	0.38 eV	A
656	6936 [c]	$1^+;0$			44	$>$0.13 eV [d]	6941	$1_{11}^+;0$	,0.025	0.43	89	0.19 eV	
928	7198	$1^+;0$			97	$>$1.3 eV	7280	$1_{12}^+;0$	,0.026	5.3	95	0.94 eV	A-B
1196	7455	$1^+;0$			94	$>$1.5 eV	7633	$1_{13}^+;0$	,0.063	64	93	0.74 eV	A-B
1370	7623	$1^+;0$			86	$>$0.5 eV	8122	$1_{14}^+;0$	,0.047	106	96	1.23 eV	B
1568	7814 [e]	$1^+;0+1$		650	81	1.7 *4* eV	8495	$1_{15}^+;0$	,0.0040	21	92	0.91 eV	C
1637	7880 [e]	$1^+;0+1$			43	8 *2* eV [f]							
	1759	$2^+;0$	0.31,0.57		100 [b]	6.0 *5* ps	1326	$2_1^+;0$	0.32,0.35		100 [b]	90 ps	A
	2661 [c]	$2^+;0$	0.0061,0.027		100 [b]	3.0 *4* ps	2588	$2_2^+;0$	0.021,0.058		100 [b]	1.6 ps	A-B
	2913 [c]	$2^+;0$	0.092,0.14		100 [b]	98 *6* fs	2749	$2_3^+;0$	0.075,0.093		100 [b]	208 fs	
	3751	$2^+;0$	0.24,0.34		83	32 *8* fs	3923	$2_4^+;0$	0.15,0.23		77	17 fs	A
	5495	$2^+;0$			97	$<$7 fs	5288	$2_5^+;0$	0.00090,0.0079		92	5.1 fs	A
	5849	$2^+;0$			75	14 *8* fs	5453	$2_6^+;0$	0.00042,0.0085		52	11.0 fs	B
390	6680	$2^+;0$	0.068,0.036 [i]		79	0.22 *2* eV	6003	$2_7^+;0$	0.049,0.048	0.98	82	0.063 eV	A
567	6852 [e]	$2^+;0+1$			7	0.76 *8* eV [g]	6149	$2_8^+;0$	0.015,0.010	9.89	74	0.058 eV	A
593	6876 [e]	$2^+;1$			3.2	0.52 *4* eV [g]							
723	7001 [c]	$2^+;0$			78	0.44 *4* eV [g]	6688	$2_9^+;0$	0.012,0.0037	31	94	0.31 eV	A-B
819	7093 [c]	$2^+;0$			74	0.12 *4* eV [g]	7114	$2_{10}^+;0$	0.0017,0.00029	9.4	69	0.067 eV	
1135	7397 [c]	$2^+;0$		45	55	0.25 *2* eV	7469	$2_{11}^+;0$	0.00090,0.058	72	92	0.42 eV	B
1302	7558 [c]	$2^+;0$		170	83	0.9 *2* eV	7527	$2_{12}^+;0$	0.000037,0.034	59	91	0.37 eV	
1622	7865	$2^+;0(+1)$		6600	35	0.7 *2* eV	7686	$2_{13}^+;0$	0.012,0.010	1950	84	0.15 eV	A-B
1771	8008	$2^+;0$		760	52	0.46 *8* eV	8039	$2_{14}^+;0$	0.0023,0.0077	595	94	0.34 eV	B-C
	417	$3^+;0$	0.77,		100 [b]	1.80 *5* ns	712	$3_1^+;0$	0.64,0.067		100 [b]	115 ps	A
	2365 [c]	$3^+;0$	0.032,0.28		100 [b]	1.4 *3* ps	2121	$3_2^+;0$	0.029,0.32		100 [b]	8.4 ps	A
	2545 [c]	$3^+;0$	0.052,0.21		100 [b]	1.00 *25* ps	2325	$3_3^+;0$	0.0015,0.15		100 [b]	1.2 ps	
	3074	$3^+;0$	0.0065,0.039		83	280 *45* fs	3069	$3_4^+;0$	0.00035,0.037		87	169 fs	A
	3596 [c]	$3^+;0$	0.033,0.10		92	24 *4* fs	3357	$3_5^+;0$	0.0072,0.041		96	15 fs	A
	3681 [c]	$3^+;0$	0.065,0.36		94	12 *2* fs	3656	$3_6^+;0$	0.035,0.095		85	76 fs	
	3963	$3^+;0$	,0.059		70	54 *7* fs	4103	$3_7^+;0$	0.013,0.22		77	38 fs	A
	4349	$3^+;0$			94	13 *4* fs	4380	$3_8^+;0$	0.00032,0.042		90	10 fs	A
	4952	$3^+;0$			83	14 *4* fs	5014	$3_9^+;0$	0.0015,0.040		71	16 fs	A
	5883	$3^+;0$			70	$<$17 fs	6241	$3_{10}^+;0$	0.00067,0.011		93	2.9 fs	B
	6280	$3^+;0$			90	$<$20 fs	6589	$3_{11}^+;0$	0.00092,0.012		80	7.3 fs	B
515	6801	$3^+;0$			73	$>$0.08 eV	6697	$3_{12}^+;0$	0.000070,0.0095	0.036	98	0.56 eV	B
775	7051 [c]	$3^+;0$			86	0.23 *2* eV [g]	7128	$3_{13}^+;0$	0.011,0.017	45	98	0.54 eV	A
881	7153 [c]	$3^+;0$		90.0	91	0.56 *6* eV	7194	$3_{14}^+;0$	0.0049,0.0062	43.0	91	0.16 eV	
1205	7464 [e]	$3^+;0+1$		80.0	24	0.76 *10* eV [g]	7450	$3_{15}^+;0$	0.0042,0.015	218	95	0.29 eV	A-B
1237	7495 [e]	$3^+;0+1$			16	1.2 *2* eV							
1525	7772	$3^+;0$			76	0.42 *6* eV [g]	7883	$3_{16}^+;0$	0.042,0.0014	5110	90	0.43 eV	A
1632	7874	$3^+;0$		1200	80	1.0 *1* eV	8026	$3_{17}^+;0$	0.0000001,0.016	96.8	97	0.86 eV	B
	2069	$4^+;0$			100 [b]	450 *70* fs	2303	$4_1^+;0$	,0.025		100 [b]	550 fs	A

TABLE VII. *(Continued).*

Experiment							Shell model						
E_R (keV)	E_x (keV)	$J^\pi;T$	S $\ell=0+2$	Γ_p (eV)	$M1_{IV}$ decay	τ_m or Γ_γ	E_x (keV)	$J_n^\pi;T$	S $\ell=0+2$	Γ_p (eV)	$M1_{IV}$ decay	τ_m or Γ_γ	
	3675	$4^+;0$			100 [b]	225 *30* fs	3309	$4_2^+;0$	,0.16		100 [b]	480 fs	A
	4206	$4^+;0$			100 [b]	90 *15* fs	4052	$4_3^+;0$	,0.064		100 [b]	172 fs	A
	4773	$4^+;0$	,0.15		100 [b]	118 *17* fs	4722	$4_4^+;0$	,0.026		100 [b]	156 fs	A
	5245	$4^+;0$	,0.23		49	17 *4* fs	5211	$4_5^+;0$	,0.10		73	19 fs	A
	5513	$4^+;0$	,0.36		38	51 *6* fs	5348	$4_6^+;0$	,0.45		31	49 fs	A
(38)	6343	4;0	,0.0071 [i]		71	<8 fs	6031	$4_7^+;0$	,0.0075		55	18 fs	A
							6667	$4_8^+;0$	,0.070		28	10 fs	
1025	7291	$4^+(3^+);0$		55.0	29	0.34 *3* eV	7265	$4_9^+;0$	,0.00053	0.21	54	0.084 eV	B
1164	7425	$4^+;0$		65.0	55	0.27 *3* eV	7402	$4_{10}^+;0$	,0.014	12.0	69	0.088 eV	A-B
1337	7592 [c]	$4^+(3^+);0$		17.0	62	0.11 *3* eV	7557	$4_{11}^+;0$	,0.0062	12.0	84	0.15 eV	A
1587	7832 [c]	$4^+;0$		110	25	0.91 *11* eV	7651	$4_{12}^+;0$	,0.015	74.0	80	0.23 eV	
	0	$5^+;0$	,0.77				[0]	$5_1^+;0$	,1.05				
	3403	$5^+;0$			100 [b]	96 *18* fs	3422	$5_2^+;0$	,0.0095		100 [b]	159 fs	A
	4941	$5^+;0$			100 [b]	35 *8* fs	4481	$5_3^+;0$	,0.014		100 [b]	137 fs	A
	5488 [c]	$5^+(4^-);0$			100 [b]	25 *8* fs [d]	5533	$5_4^+;0$	,0.00002		100 [b]	80 fs	B
	5569 [c]	(4,5);0			100 [b]	[d]	5579	$5_5^+;0$	,0.00007		100 [b]	85 fs	
(135)	6436 [c]	$5^+;0$	$,\leqslant 0.0021$ [i]		100 [b]	<24 fs	6069	$5_6^+;0$	,0.012		100 [b]	12 fs	A
198	6496 [c]	$5^+;0$	,0.021 [i]		100 [b]	<12 fs	6321	$5_7^+;0$	,0.041		100 [b]	22 fs	
304	6598 [c]	$5^+;0$			100 [b]		6449	$5_8^+;0$	,0.00050		100 [b]	33 meV	A
738	7015	$5^+;0$			67	>34 meV	7017	$5_9^+;0$	,0.010	0.43	82	68 meV	
1103	7366	$5^+;0$			75	>25 meV	7167	$5_{10}^+;0$	,0.000010	0.0062	70	85 meV	A
1342	7596	$5^+;0$			65	>0.26 eV	7291	$5_{11}^+;0$	,0.00080	1.58	63	91 meV	B
							7886	$5_{12}^+;0$	,0.0075		38	95 meV	
	3508	$6^+;0$			100 [b]	24 *5* fs	3334	$6_1^+;0$			100 [b]	38 fs	A
	6120	$(4\text{-}6^+);0$			100 [b]	15 *5* fs		6176	$6_2^+;0$		100 [b]	34 fs	A
(530)	6816	$(4\text{-}6^+);0$			100 [b]	<22 fs		6521	$6_3^+;0$		100 [b]	33 fs	A
								7479	$6_4^+;0$		100 [b]	12 meV	
1680	7921	$(5,6)^+;0$			100 [b]	>31 meV		7940	$6_5^+;0$		100 [b]	31 meV	B
	3922	$7^+(5^+);0$			100 [b]	28 *6* fs		3750	$7_1^+;0$		100 [b]	48 fs	A
(405)	6695 [h]	$7^{(+)};0$			40			6243	$7_2^+;0$		100 [b]	54 fs	A

[a] See Table VI for explanation of symbols used in column headings.

[b] All $M1$ and $E2$ transitions (not only $M1_{IV}$) have been used in the branching comparison; for $T=0\rightarrow 0$, $|\Delta J|=1$, transitions the theoretical $M1_{IS}$ and $E2_{IS}$ strengths have been added.

[c] Configuration-mixed doublet.

[d] For the branching comparison τ_m^{expt} (or Γ_γ^{expt}) has been taken equal to τ_m^{SM} (or Γ_γ^{SM}).

[e] Isospin-mixed doublet.

[f] See Sec. IV A.

[g] For these $\ell=0$ resonances we assume $\Gamma_p \gg \Gamma_\gamma$, such that the (p,γ) yield can be used to obtain Γ_γ.

[h] Previously unobserved level from Ref. [34].

[i] From present work (Table II).

(ii) The difference of a factor 6.8 (with $\Gamma_\gamma^{expt}=0.11\times 1.7+0.51\times 0.42=0.40$ eV) for the isospin-mixed $E_R=1568+1637$ keV doublet results from an error in Ref. [15]. For $E_R=1637$ keV the calculation of Γ_{p_0}, Γ_{p_1}, and Γ_{p_2} from $S(p,p_1)$, $S(p,p_2)$, and Γ (the values of which are given in Ref. [30]) leads to a quadratic equation in Γ_{p_0} with the solutions $\Gamma_{p_0}=3.5$ keV (given in Ref. [30]) and $\Gamma_{p_0}=185$ eV. The smaller value should have been used, which is supported by the fact that the resonance has not been seen in the (p,p_0) work of Ref. [36]. From $S(p,\gamma)=1.2$ eV we find $\Gamma_\gamma^{expt}=8.0$ eV, yielding 4.2 eV for the $M1_{IV}$ fraction of the two resonances, in reasonable agreement with the shell-model value of 2.7 eV for the $1_3^+;1$ assignment.

A comparison of experimental spectroscopic factors S and proton partial widths Γ_p with shell-model results for both $T=0$ and $T=1$ levels in ^{26}Al is presented in Sec. IV B.

B. $T=0$ $\pi=+$ states of ^{26}Al

The shell-model description of the observed $T=0$ ^{26}Al states is generally good, but there remain far more uncertainties and ambiguities compared to the $T=1$ states. The main reason for this is that there are many more $T=0$ than $T=1$ levels, such that the average $T=0$ level separation differs only little from the average error in the shell-model eigenenergies. For example, in the $E_x=5$–8 MeV region we find 21 $T=1$ and 58 $T=0$, $\pi=+$, levels. The consequence is more configuration mixing and poorer agreement for the γ-ray branching ratios. Some examples for which $E_x^{\rm expt}$ and $E_x^{\rm SM}$ agree poorly and, therefore, the correspondences are doubtful are the $0_1^+;0$, $1^+_{14-15};0$, $5^+_{10-11};0$ states and all $2^+;0$ levels above $2_5^+;0$. We note that for the $4_8^+;0$ and $6_4^+;0$ states the experimental counterparts are missing. Furthermore, it has to be remembered that γ-ray branching agreement cannot be tested for a configuration-mixed pair if the lifetime τ_m (or width Γ_γ) of one or both components is unknown (e.g., the $1_7^+;0+1_8^+;0$ doublet). In such cases $\tau_m^{\rm expt}$ (or $\Gamma_\gamma^{\rm expt}$) has been (arbitrarily) taken equal to $\tau_m^{\rm SM}$ (or $\Gamma_\gamma^{\rm SM}$). For spins $J\geqslant 3$ the $M1_{\rm IV}$, γ-decay percentages are on the average smaller than for $T=1$, since the yrast $T=1$ states are at much higher excitation energy than the yrast $T=0$ states for the same value of J [$E_x^{\rm yrast}=417$ (3^+), 2069 (4^+), and 0 keV (5^+) for $T=0$ compared to 4192 (3^+), 4705 (4^+), and 7222 keV (5^+) for $T=1$]. Therefore, we had to include the weaker γ-decay modes $M1_{\rm IS}$ and $E2_{\rm IS}$ for 15 low-energy and for 5 high-J ($6^+;0$ and $7^+;0$) levels in order to have the comparison of γ-ray branching ratios making sense.

Spectroscopic factors $S^{\rm expt}$ and $S^{\rm SM}$ are presented in Tables VI and VII. The agreement between shell-model and experimental values is reasonably good with one exception. The large deviation of a factor 18 for the $S_{\ell=0}$ value of the $E_x=3074$ keV state simply results from the uncertainty in extracting a very small $\ell=0$ contribution from a primarily $\ell=2$ transfer from the measured deuteron angular distribution. The S value for the dominant $\ell=2$ transfer agrees with the theoretical result. The ratios of experimental and shell-model spectroscopic factors are displayed in Fig. 4 for both $T=0$ and $T=1$ states. After correcting the experimental spectroscopic factors for finite-range and nonlocality effects (Sec. II B) and omitting the $E_x=3074$ keV state the average systematic deviation amounts to a factor 1.1. The average (logarithmic) scatter around this mean corresponds to a factor 1.8.

Proton partial widths Γ_p from proton elastic scattering experiments are also listed in Tables VI and VII together with the corresponding shell-model results. Although in most cases the respective values agree within factors of 2–3, there are also notable exceptions. The large discrepancies for the resonances at $E_R=1025$ and 1632 keV (factors 260 and 12, respectively) are easily explained by the fact that the shell-model spectroscopic factors for the lowest possible ℓ value (which determine the proton widths) are very small ($S^{\rm SM}\leqslant 5\times10^{-4}$). Even small admixtures from nearby states will strongly enhance the resulting proton widths $\Gamma_p^{\rm SM}$ and thus improve the agreement with experiment. The deviations for the isospin-mixed pairs $E_R=1205+1237$ keV (factor 10) and $E_R=1568+1637$ keV (factor 30) might result from systematic uncertainties in the proton elastic scattering work of

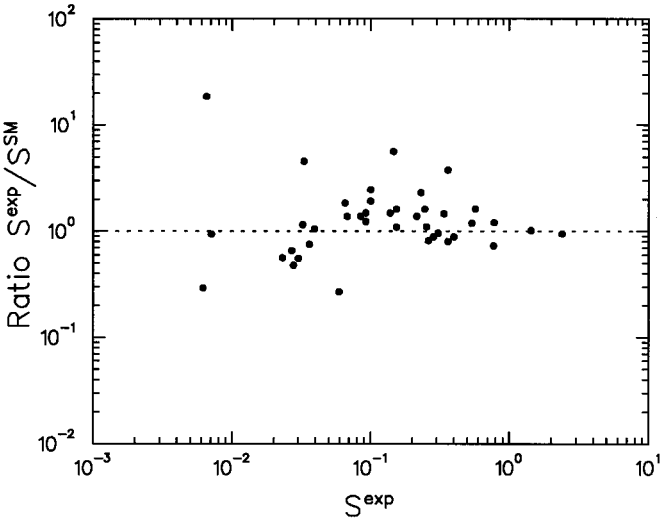

FIG. 4. Ratio of experimental and shell-model proton spectroscopic factors of ^{26}Al states. The experimental S values have been corrected for finite range and nonlocality effects.

Ref. [36]. In the first case the proximity of the broad 1239 keV resonance ($\Gamma_p^{\rm expt}=750$ eV) makes an accurate extraction of the width for $E_R=1237$ keV ($\Gamma_p^{\rm expt}=80$ eV) difficult. In the latter case we note the poor R-matrix fit to the elastic scattering data (Fig. 2 of Ref. [36]) in the region of the broad $E_R=1568$ keV resonance ($\Gamma_p^{\rm expt}=650$ keV). Furthermore, one might ask why the resonances at $E_R=1043$, 1196, 1370, and 1525 keV have not been observed in the proton elastic scattering work since the predicted proton widths ($\Gamma_p^{\rm SM}=410$, 64, 106, and 5110 eV, respectively) far exceed the experimental (lower) detection limit in Ref. [36] of ≈ 10 eV. There is indeed an indication in Fig. 1 of Ref. [36] for a resonance at $E_R=1196$ keV, although no resonance properties have been reported. The proximity of the broad $E_R=1526$ keV resonance ($\Gamma_p^{\rm expt}=5300$ eV) could have prevented the observation of $E_R=1525$ keV. Presently, we do not have a plausible explanation for the nonobservation of the $E_R=1043$ and 1370 keV resonances. These cases might indicate defects in the shell-model calculations.

The $T=0$ states at $E_x=6343$, 6436, 6496, 6551, and 6598 keV near the proton threshold in ^{26}Al possess experimentally determined spins and parities of $J^\pi=4$, 5^+, 5^+, 5^-, and 5^+, respectively (Table IV). The shell-model predicts two 4^+ and three 5^+ levels in this range of excitation energy. This makes $J^\pi=4^+$ very probable for the $E_x=6343$ keV level and leaves one shell-model 4^+ state, presumably $4_8^+;0$, unplaced. It should be noted that the stellar rates for the ^{25}Mg$+p$ reaction have been calculated previously [11–13] from proton partial widths deduced under the assumption that $J^\pi(6343)=4^-$ and $J^\pi(6436)=4^-$. The astrophysical consequences of our new J^π assignments are discussed in Sec. VI.

V. ISOSPIN TRIPLET ($T=1$) STATES IN $A=26$ NUCLEI

A. Shell-model and analog-state assignments

In this section we present new shell-model and analog assignments of $T=1$ states in ^{26}Mg, ^{26}Al, and ^{26}Si which

will be used in Sec. VII for the calculation of stellar reaction rates for ^{25}Al$(p,\gamma)^{26}$Si. The present results are shown in Table VIII.

In addition to the information given in [30] we have also taken into account more recent experimental work concerning ^{26}Mg levels: (i) the ^{25}Mg(n,γ) work of Ref. [46] provides more accurate E_x values and γ-ray branching ratios for many levels; (ii) the ^{27}Al$(d,{}^3$He) measurements of Ref. [47] with good resolution and statistics yield ℓ values for several levels; (iii) the ^{26}Mg(e,e') experiments of Refs. [48,49] determine J^π values for more than 30 states. New (accepted) values for spins and parities of ^{26}Mg states are indicated in Table VIII. We note that, by considering the 6852+6876 keV $2^+;0+1$ doublet in ^{26}Al as T mixed rather than configuration mixed (as in Ref. [30]), some ^{26}Mg and ^{26}Al 2^+ states have obtained different shell-model assignments. As another consequence, the $1_2^+;1$ state in ^{26}Mg, still considered missing in Ref. [30], can now be identified with the $E_x=6634$ keV, $J^\pi=(0-4)^+$, level.

The available experimental information on ^{26}Si levels is largely based on studies of the two-nucleon transfer reactions ^{24}Mg$({}^3$He,$n)$ [50,51] and ^{28}Si(p,t) [52]. We have also compared the $({}^3$He,$n)$ data with experimental results for the ''mirror'' reaction ^{24}Mg$(t,p)^{26}$Mg [53]. The shell-model and analog-state assignments for the lowest six ^{26}Si levels seem to be established. The states at $E_x=1796$ (2^+), 2783 (2^+), 3332 (0^+), 3756, 4138 (2^+), and 4183 keV correspond to the shell-model states of 2_1^+, 2_2^+, 0_2^+, 3_1^+, 2_3^+, and 4_1^+, respectively. The levels at 3842 and 4093 keV reported by Ref. [54] have been omitted since their existence is not well established. We assign the 4446 keV state which is weakly populated in the two-nucleon transfer work to the unnatural-parity level 3_2^+. It is shown in the $({}^3$He,$n)$ work [50] that the angular distribution leading to the 4806 keV state can only be described assuming three components with total orbital angular momentum transfers of $L=0+2+4$. This triplet has been assigned in the present work to shell-model states of 2_4^+, 4_2^+, and 0_3^+. The 5330 keV (4^+) level corresponds presumably to 4_3^+. The states at 5229 and 5562 keV which have been observed only in the (p,t) reaction are assigned to 2_5^+ and 1_1^+, respectively. The $({}^3$He,$n)$ angular distribution data leading to $E_x=5940$ keV could only be described [50] using two components with $L=0+4$. This doublet probably corresponds to shell-model states of 4_4^+ and 0_4^+. Furthermore, from the comparison of particle spectra measured in the mirror reactions ^{24}Mg$({}^3$He,$n)$ and ^{24}Mg(t,p) it follows that the four ^{26}Si states at 6350 (2^+), 6470, 6789, and 6880 keV very likely correspond to the ^{26}Mg levels at 6745 (2^+), 6878 (3^-), 7063 (1^-), and 7348 (3^-). Therefore, the ^{26}Si state at 6470 keV presumably has negative parity, although a 0^+ assignment has been reported in the $({}^3$He,$n)$ work of Ref. [50]. The experimental angular distribution measured in that work is shown in Fig. 3(d) together with DWBA fits for $L=0$, 1, and 3 transfers. As in Ref. [50] we have used the Bayman-Kallio method for the construction of a total microscopic form factor from two single-particle form factors. This procedure is implemented in the program DWUCK4. Since the code cannot handle two-particle transfers leading to unbound final states, we have bound each proton by 50 keV. We have used the same optical-model and form factor parameters as in Ref. [50]. The calculations have been performed using single-particle form factors of $2s_{1/2}^2$ $(L=0)$, $1d_{3/2}2p_{1/2}$ $(L=1)$, and $1d_{3/2}2p_{3/2}$ $(L=3)$ although the shapes of the calculated angular distributions are relatively insensitive to the particular choice of form factors. It can be seen from Fig. 3(d) that at angles $\theta_{\rm c.m.}<40°$ the $L=1$ transfer describes the data as well as the $L=0$ transfer, while a 3^- assignment is clearly excluded. The observed structure at $\theta_{\rm c.m.}>40°$ cannot be described by a particular L transfer and may arise from an unresolved state or a contaminant. Therefore, we assign a spin and parity of 1^- to the 6470 keV state. Our conclusions are supported by the fact that the $({}^3$He,$n)$ angular distribution for the unresolved 6789+6880 keV doublet in Ref. [51] is well described assuming an $L=3$ transfer. Further, we assign the levels at 7150 (2^+) and 7489 (2^+) keV to the shell-model states of 2_7^+ and 2_8^+, respectively. It should be noted at this point that far less experimental information is available on ^{26}Si states compared to the other two members of the isospin triplet and, therefore, the level assignments are not as well established in this case. However, our results are more consistent with existing experimental data than the previous assignments of Refs. [30,51].

B. Coulomb displacement energies

Coulomb displacement energy calculations have been performed in the present work for the mirror pair ^{26}Mg$-^{26}$Si, in order to support our ^{26}Si level assignments and also to estimate the excitation energies of the unobserved 3_3^+, 1_2^+, and 4_5^+ states in ^{26}Si (Table VIII). In order to calculate ^{26}Si level energies from measured excitation energies of ^{26}Mg states we have employed three different methods: an empirical estimate, a single-particle potential model, and a hybrid model.

For the empirical estimate we have collected all experimentally measured excitation energy differences of $T=1$ mirror states in even-A nuclei in the mass $A=22$–34 region. The $A=22$, 24, 26, 30, and 34 mirror pairs each contribute at most five cases, but the situation is much better for $A=28$ and 32. Altogether there are about 50 cases for which we have plotted in Fig. 5 the difference Δ in excitation energies of corresponding levels in $T_z=-1$ (proton-rich) and $T_z=+1$ (neutron-rich) nuclei. The energies of $T=1$ states in $T_z=0$ nuclei have not been considered for comparison purposes because of possible isospin mixing giving rise to isospin doublets and additional shifts. It can be seen from Fig. 5 that on the average the differences Δ are negative which is well known. There is also a tendency for the absolute differences to increase with excitation energy according to the relation

$$\Delta_{\rm av}=-0.025E_x(T_z=+1), \tag{4}$$

where E_x is in units of keV. The scatter around this average amounts to 41 keV. These 50 cases relate to $\pi=+$ states only. It is well known that for $\pi=-$ states the energy shifts are much larger. Very few negative parity levels have been found in $T_z=-1$ nuclei, but the large shifts can be demonstrated, e.g., by comparing corresponding $\pi=-$ levels in ^{26}Mg and ^{26}Al. For six pairs the quantity $[E_x(^{26}\text{Al})-E_x(^{26}\text{Mg})-228$ keV$]$ amounts to about -170 keV. An ex-

TABLE VIII. Isospin triplet states ($T=1$) in $A=26$ nuclei. [a]

^{26}Mg		^{26}Al		^{26}Si		Shell model [c]	
E_x (keV)	J^π	E_x (keV)	$J^\pi;T$ [b]	E_x (keV)	J^π [g]	E_x (keV)	$J^\pi;1$
0	0^+	228	$0^+;1$	0	0^+	[0]	0_1^+
1809	2^+	2070	$2^+;1$	1796	2^+	1929	2_1^+
2938	2^+	3160	$2^+;1$	2783	2^+	3153	2_2^+
3589	0^+	3754	$0^+;1$	3332	0^+	3681	0_2^+
3941	3^+	4192	$3^+;1$	3756		3921	3_1^+
4332	2^+	4548	$2^+;1$	4138	2^+	4541	2_3^+
4350	3^+	4599	$3^+;1$	4446		4511	3_2^+
4318	4^+	4705	$4^+;1$	4183		4533	4_1^+
4900	4^+	5132	$4^+;1$	4806		4932	4_2^+
4834	2^+	5142	$2^+;1$	4806		5000	2_4^+
4972	0^+	5195	$0^+;1$	4806		5204	0_3^+
5291	2^+	5545	$2^+;1$	5229		5404	2_5^+
5474	4^+	5726	$4^+;1$	5330	4^+	5473	4_3^+
5716	4^+	5924	$4^+;1$	5940		6009	4_4^+
5690	1^+ [d]	6028	$1^+;1$	5562		5833	1_1^+
6125	3^+	6364	$3^+;1$			6268	3_3^+
6256	0^+	6414	$0^+;1$	5940	0^+	6062	0_4^+
6634	$(0\text{-}4)^+$ [d]	6802	$1^+(1^-,2^-);0+1$			6798	1_2^+
6622	4^+	6818	$4^+;1$			6777	4_5^+
6745	2^+	6852	$2^+;0+1$	6350	2^+	6647	2_6^+
		6876	$2^+;1$				
6878	3^-	6964	$3^-;1$	6789			
7063	1^-	7086	$1^-;1$	6470			
6978	5^+	7222	$5^+;1$			7038	5_1^+
7261	$(2,3)^-$	7254	$2^-;1$				
7100	2^+	7308	$2^+;1$	7150	2^+	6843	2_7^+
7282	4^-	7348	$4^-;1$				
		7410	$4^-;1$				
7349	3^- [f]	7399	$3^-;1$	6880			
		7440 [h]	(0-2);1				
7242	3^+ [d, e]	7464	$3^+;0+1$			7282	3_4^+
		7495	$3^+;0+1$				
7543	2^- [e]	7497	$2^-;0+1$				
		7540	$2^-;1$				
7369	2^+ [e]	7561	$2^+;1$	7489	2^+	7093	2_8^+
7395	5^+	7628	$5^+;1$			7465	5_2^+
7428	$(0,1)^+$ [f]	7814	$1^+;0+1$			7721	1_3^+
		7880	$1^+;0+1$				
7677	4^+ [e]	7891	$4^+;1$			7411	4_6^+
7724	3^+ [d, e]	7939	$3^+;1$			7602	3_5^+
7773	4^+ [e]	7953	$4^+;1$			7941	4_7^+
7816	$(2,3)^+$	7982	$2^+;1$			7473	2_9^+
7694	1^- [d, f]	8001	$1^-;1$				
7953	5^-	8011	$5^-;1$				
		8067	$5^-;1$				
7840 [h]	2^+	8064 [h]	$2^+;1$				

[a] Experimental excitation energies and J^π values adopted from Ref. [30] unless indicated otherwise.

[b] See also Table III.

[c] See also Sec. IV A; shell-model excitation energies are given relative to the $0_1^+;1$ state.

[d] Recent experimental information from transfer work [47] has been taken into account.

[e] Recent experimental information from electron inelastic scattering work [48,49] has been taken into account.

[f] For these levels the electron inelastic scattering work of Ref. [49] yields $J^\pi(7349)=1^-$, $J^\pi(7428)=2^+$, and $J^\pi(7694)=3^-$; however, the correspondence with ^{26}Al states clearly proves J^π-values of 3^-, 1^+, and 1^-, respectively.

[g] Listed are only those J^π values which have been obtained from unambiguous DWBA descriptions of (^{3}He,n) data [50,51].

[h] Intruder states.

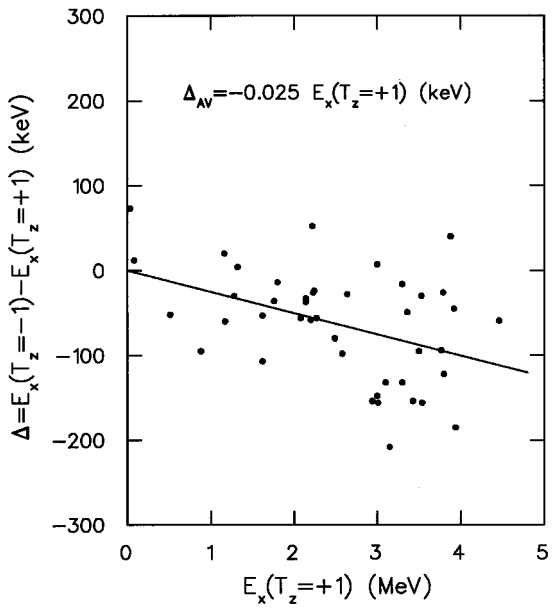

FIG. 5. Excitation energy differences of $T=1$ mirror states in even-A nuclei in the mass $A=22-34$ region. The absolute differences increase linearly with excitation energy.

ception is the ^{26}Al 1^-;1 level at 8001 keV with the ^{26}Mg parent located at 7694 keV. The change of sign for the Coulomb energy shift can be explained by a hole in the $1p$ shell rather than a particle in the $2p$ shell. Fortunately, negative parity levels are negligible for the ^{25}Al$(p,\gamma)^{26}$Si reaction rates in the stellar temperature range of interest in the present work (Sec. VII) since none of these are expected within ≈ 1 MeV above the proton threshold. Predicted excitation energies of ^{26}Si levels deduced from the known ^{26}Mg mirror state energies using Eq. (4) are listed in column 2 of Table IX.

In the single-particle potential model it is assumed that the ^{26}Si (^{26}Mg) states can be described by the motion of a proton (neutron) around a core consisting of the ^{25}Al (^{25}Mg) ground state. For the interaction of the neutron with the ^{25}Mg core a Woods-Saxon potential with parameters $r_0=1.25$ fm and $a=0.65$ fm plus a spin-orbit potential of 25 times the Thomas term has been used (see also Table I). The well depth of the Woods-Saxon potential was chosen to reproduce the excitation energy in ^{26}Mg. The energy of the ^{26}Si mirror level was then calculated for the same potential depth including a Coulomb field of a uniform spherical charge of radius $r_0A^{1/3}$. For each positive parity level below $E_x\approx 7$ MeV the resulting single-orbit shifts ($2s_{1/2}$, $1d_{3/2}$, $1d_{5/2}$) have been corrected for the shift of the $1d_{5/2}$ ground state and weighted by the corresponding single-particle spectroscopic factors. The latter values were obtained from a shell-model calculation (Sec. IV). The ^{26}Mg level energies have been corrected by the calculated total Coulomb shifts and the resulting ^{26}Si excitation energies are listed in column 3 of Table IX. We note that this model obviously neglects the possibility of single-particle states built onto excited cores.

A hybrid model for the calculation of Coulomb shifts has been adopted from Ref. [55] to which the reader is referred for details. In brief, shell-model calculations of ^{26}Mg and ^{26}Al excitation energies have been performed for which the empirical isospin-nonconserving interactions of Ormand and Brown [56] were added to the W interaction. The Ormand-Brown interaction matrix elements have been adjusted to reproduce experimental isobaric mass shifts and should in principle account for multiparticle effects of the Coulomb displacement energies. However, the Thomas-Ehrman shift [57,58] is neglected in the calculations since the Ormand-Brown interactions have been derived using harmonic-oscillator radial wave functions. This shift was taken into account additionally using a single-particle (Woods-Saxon) potential model. The resulting single-orbit shifts for both ground state and excited cores are multiplied by the corresponding calculated spectroscopic factors and are added together yielding a total Thomas-Ehrman shift. The measured ^{26}Mg excitation energies were corrected for both the shell-model excitation energy differences and the Thomas-Ehrman shifts. The resulting excitation energies of the ^{26}Si mirror states are presented in column 4 of Table IX.

TABLE IX. Coulomb displacement energies (in keV) for ^{26}Mg-^{26}Si.

	$E_x^{\rm calc}(^{26}{\rm Si})$					
$J^\pi_{\rm SM}$	EE [a]	SPM [b]	HYB [c]	$E_x^{\rm av}$ [d]	$E_x^{\rm expt}(^{26}{\rm Si})$ [e]	$(E_x^{\rm expt}-E_x^{\rm av})$
0_1^+	0	0	0	0	0	
2_1^+	1764	1734	1839	1794	1796	+2
2_2^+	2864	2736	2856	2833	2783	−50
0_2^+	3499	3423	3531	3499	3332	−167
3_1^+	3842	3791	3838	3838	3756	−82
4_1^+	4210	4280	4450	4328	4183	−145
2_3^+	4224	4091	4290	4216	4138	−78
3_2^+	4241	4077	4297	4220	4446	+226
2_4^+	4713	4526	4933	4739	4806	+67
4_2^+	4778	4821	4915	4853	4806	−47
0_3^+	4848	4718	4997	4869	4806	−63
2_5^+	5159	5165	5249	5205	5229	+24
4_3^+	5337	5266	5381	5342	5330	−12
1_1^+	5548	5493	5830	5638	5562	−76
4_4^+	5573	5409	5816	5614	5940	+326
3_3^+	5972	5813	6080	5970		
0_4^+	6100	5901	5986	6010	5940	−70
1_2^+	6468	6322	6524	6452		
4_5^+	6456	6232	6620	6451		
2_6^+	6576	6259	6625	6501	6350	−151
2_7^+	6922	6593	6980	6846	7150	+304
5_1^+	6803	6549		6741		

[a]From empirical estimate.
[b]From single-particle model.
[c]From hybrid model.
[d]Average values (see text).
[e]Experimental excitation energies in ^{26}Si (Table VIII).

The estimated ^{26}Si excitation energies are compared to the newly proposed (experimental) ^{26}Si level scheme (column 6 of Table IX). For the three different methods described above one finds average deviations of $(E_x^{\rm expt}-E_x^{\rm calc})_{\rm av}=+9$, $+120$, and -85 keV, respectively. The calculated energies have been corrected for these systematic

deviations and the average is listed in column 5 of Table IX. For the latter values the average absolute deviation amounts to $|E_x^{\rm expt}-E_x^{\rm calc}|_{\rm av}=110$ keV, which is not surprising in view of the theoretical and experimental uncertainties involved. We expect the unobserved ^{26}Si levels of 3_3^+, 1_2^+, and 4_5^+ at $E_x=5.97$, 6.45, and 6.45 MeV, respectively, with an estimated uncertainty of about 0.1 MeV.

VI. STELLAR REACTION RATES FOR ^{25}Mg+p

The stellar reaction rates $N_A\langle\sigma v\rangle$ of ^{25}Mg$(p,\gamma)^{26}$Al can have contributions from narrow resonances, the high-energy wing of the $E_R=-25.7$ keV subthreshold resonance, the direct capture into final ^{26}Al states, and the summed low-energy wings of resonances located at higher energies. Calculations have shown [18,59] that for stellar temperatures $T\geqslant 0.01$ GK the last three contributions can be neglected.

The reaction rate (in units of reactions $\mathrm{s}^{-1}\,\mathrm{mol}^{-1}\,\mathrm{cm}^3$) for isolated narrow resonances is given as a function of temperature T_9 (in units of GK) by the expression [60]

$$N_A\langle\sigma v\rangle=1.54\times10^{11}(\mu T_9)^{-3/2}\sum_i f_i\omega\gamma_i\exp\left(-11.605\frac{E_i}{T_9}\right), \tag{5}$$

where the reduced mass μ is in amu and the strengths $\omega\gamma_i$ and center-of-mass energies E_i of the resonances are in MeV; f_i denotes the γ-ray branching ratios to the ground state of ^{26}Al. For stellar temperatures of greatest interest here ($T\leqslant 2.0$ GK), all experimentally observed resonances with $E_i\leqslant 1455$ keV were considered. All resonance energies E_i have been calculated from the E_x values reported in [30] using $Q_{p\gamma}=(6306.55\pm0.06)$ keV [61]. For the γ-ray branchings to the ^{26}Al ground state we have used the values from Table IV of Ref. [18], except for the resonances at $E_R=198$, 254, and 304 keV, for which f_i has been calculated from recently measured [11] primary γ-ray branching ratios (new values are $f_i=0.66$, 0.76, and 0.79, respectively). Measured resonance strengths $\omega\gamma_i$ for $E_R=198$–317 keV were taken from Ref. [11]. For higher-lying resonances the values of Ref. [15], determined relative to $E_R=591+593$ keV from Ref. [62], were adopted. The different data sets overlap at the $E_R=317$ keV resonance and yield consistent values within the quoted experimental uncertainties.

For the threshold states at $E_x=6343$–6436 keV it has been shown [16] that $\Gamma_\gamma/\Gamma\approx 1$. Therefore, the strengths $\omega\gamma$ of the corresponding resonances at $E_R=38$–135 keV are given by

$$\omega\gamma\approx\omega\Gamma_p, \tag{6}$$

and thus can be calculated from the average proton widths deduced in the present work. As already noted, for a few threshold states either an unambiguous J^π value could not be determined experimentally or only an upper limit for the proton width Γ_p has been obtained from the (^{3}He,d) data (Secs. II B and III). Therefore, we have calculated upper and lower limits for their contributions to the reaction rates, based on the largest and smallest possible values of Γ_p. The $\omega\gamma$ values used for the calculation of these limits are listed in Table III.

Lower and upper limits on the total reaction rates for the nucleosynthesis of the ^{26}Al ground state via ^{25}Mg+p are presented in Table X. Total rates (solid line) and individual contributions (dashed lines) are displayed in Fig. 6(a). The observed resonances with $E_R\geqslant 198$ keV determine the stellar rates for temperatures $T>0.15$ GK, whereas the $E_R=60$ and 96 keV resonances dominate the rates for $T=0.02-0.15$ GK. The upper and lower limits for the ^{25}Mg+p reaction rates deviate only by negligible amounts in the astrophysically important temperature range $T>0.02$ GK. The resonance at $E_R=135$ keV is too weak to influence the reaction rates appreciably. We also note that the $E_R=38$ and 112 keV resonances are unimportant at these temperatures. Only at lower stellar temperatures of $T<0.015$ GK does the $E_R=38$ keV resonance dominate the stellar rates. The shell-model prediction (Sec. IV) of $J^\pi=4^+;0$ yields a strength of $\omega\gamma=4.5\times10^{-22}$ eV for this resonance, compared to $\omega\gamma<2.4\times10^{-20}$ eV resulting from the previous assignment $J^\pi=4^-$ (Table III). However, at these low stellar temperatures contributions to the reaction rates other than from narrow resonances also have to be taken into account [18,59].

We attribute an uncertainty of a factor 1.5 to the reaction rates at temperatures $T=0.02$–0.07 GK, which are dominated by the $E_R=60$ keV resonance. For temperatures $T=0.07$–0.15 GK the reaction rates are determined by the contributions of the $E_R=96$ keV resonance. The reader should be aware of the fact that in this range the stellar rates of the present work could be systematically lower by a factor of 2, or possibly more, depending on the magnitude of multiple-step contributions to the population of the corresponding state at $E_x=6399$ keV in the ^{25}Mg(^{3}He,d)^{26}Al reaction (Sec. II B). For temperatures above $T=0.15$ GK the uncertainties are determined by the experimental errors of the $\omega\gamma_i$ values (about $\pm20\%$). In addition, Table X lists values for the ground-state branching ratio f_0 versus stellar temperature T which have been determined using the method described in Ref. [18]. The reaction rates for forming the isomeric state ^{26}Al^m via ^{25}Mg+p are then obtained by multiplying the presented $N_A\langle\sigma v\rangle$ values by the factor $(1-f_0)/f_0$.

The previously derived reaction rates of Champagne *et al.* [12] and Rollefson *et al.* [13] are listed in Table X and are compared in Fig. 6(b). A maximum deviation of a factor of 3 occurs at $T=0.1$ GK. The ratio of our stellar rates and the previous results are also shown in Fig. 6(b). The present reaction rates deviate a factor of 2 at $T=0.1$ GK from the values given in Ref. [13], but do agree within 40% with the results of Ref. [12] at temperatures $T>0.02$ GK. We note that the reaction rates for ^{25}Mg+p are now based on an improved analysis of all available experimental data.

VII. STELLAR REACTION RATES FOR ^{25}Al+p

The stellar rates for the ^{25}Al$(p,\gamma)^{26}$Si reaction were calculated using the new shell-model and analog assignments of ^{26}Si states presented in Sec. V.

The contribution of narrow resonances to $N_A\langle\sigma v\rangle$ was calculated by using Eq. (5) (with $f_i=1$). For stellar temperatures of $T<1.5$ GK it is sufficient to consider resonances located within about 1 MeV of the proton threshold in ^{26}Si ($Q_{p\gamma}=5518$ keV). It is apparent from Table VIII that in this

TABLE X. Stellar reaction rates $N_A\langle\sigma v\rangle$[a,b] for $^{25}\mathrm{Mg}(p,\gamma)^{26}\mathrm{Al}^0$.

T (GK)	Low [c]	High [d]	[e]	[f]	f_0 [g]
0.01	4.19×10^{-34}	7.74×10^{-31}	3.47×10^{-34}		0.79
0.015	1.02×10^{-24}	1.68×10^{-24}	8.63×10^{-25}		0.81
0.02	4.42×10^{-20}	4.47×10^{-20}	3.79×10^{-20}	3.9×10^{-20}	0.81
0.03	1.61×10^{-15}	1.61×10^{-15}	1.39×10^{-15}	1.4×10^{-15}	0.81
0.04	2.75×10^{-13}	2.75×10^{-13}	2.39×10^{-13}	2.4×10^{-13}	0.81
0.05	6.17×10^{-12}	6.17×10^{-12}	5.27×10^{-12}	6.1×10^{-12}	0.81
0.06	5.83×10^{-11}	5.83×10^{-11}	4.78×10^{-11}	7.1×10^{-11}	0.82
0.07	3.53×10^{-10}	3.54×10^{-10}	2.76×10^{-10}	5.2×10^{-10}	0.83
0.08	1.54×10^{-9}	1.55×10^{-9}	1.16×10^{-9}	2.6×10^{-9}	0.84
0.09	5.15×10^{-9}	5.19×10^{-9}	3.81×10^{-9}	9.8×10^{-9}	0.84
0.1	1.42×10^{-8}	1.44×10^{-8}	1.05×10^{-8}	2.9×10^{-8}	0.83
0.15	5.49×10^{-6}	5.51×10^{-6}	5.94×10^{-6}	5.8×10^{-6}	0.84
0.2	1.11×10^{-3}	1.11×10^{-3}	1.23×10^{-3}	1.0×10^{-3}	0.86
0.3	2.44×10^{-1}	2.44×10^{-1}	2.51×10^{-1}	2.2×10^{-1}	0.84
0.4	3.67×10^{0}	3.67×10^{0}	3.32×10^{0}	3.3×10^{0}	0.83
0.5	1.93×10^{1}	1.93×10^{1}	1.75×10^{1}	1.7×10^{1}	0.81
0.6	5.98×10^{1}	5.98×10^{1}	5.43×10^{1}		0.80
0.7	1.36×10^{2}	1.36×10^{2}	1.24×10^{2}		0.79
0.8	2.55×10^{2}	2.55×10^{2}	2.32×10^{2}		0.77
0.9	4.18×10^{2}	4.18×10^{2}	3.81×10^{2}		0.76
1.0	6.24×10^{2}	6.24×10^{2}	5.71×10^{2}		0.75
1.5	2.15×10^{3}	2.15×10^{3}	1.95×10^{3}		0.72
2.0	4.15×10^{3}	4.15×10^{3}	3.68×10^{3}		0.70

[a]Reaction rates for the population of the ^{26}Al ground state in units of reactions $\mathrm{s}^{-1}\ \mathrm{mol}^{-1}\ \mathrm{cm}^3$; in order to calculate the stellar rates for the population of the isomeric state the presented values of $N_A\langle\sigma v\rangle$ have to be multiplied by the factor $(1-f_0)/f_0$.

[b]Contributions of narrow resonances only; for $T\leqslant0.01$ GK additional contributions from the direct capture process, the $E_R=-26$ keV subthreshold resonance, and the low-energy tails of higher-lying resonances have to be taken into account [18,59].

[c]Contribution of all measured (p,γ) resonances and $E_R=60$, 96, 112 keV.

[d]Sum of column 2 and maximum possible contribution from $E_R=38$ and 135 keV (Table IV).

[e]Calculated from analytic expression given on p. 393 of Ref. [12].

[f]From Table IV of Ref. [13].

[g]Gamma-ray branching ratio for the population of the ^{26}Al ground state.

range of excitation energy only positive parity states are expected. Resonance energies E_R were calculated from the excitation energies listed in Table VIII for experimentally observed levels (with typical errors of ±25 keV). For the unobserved shell-model states of 3_3^+, 4_5^+, and 1_2^+ we used the predictions of Coulomb displacement energy calculations, where the uncertainties involved amount to about 100 keV (Table IX and Sec. V B). The resonance strengths $\omega\gamma$ are determined by the proton and γ-ray partial widths Γ_p and Γ_γ. Proton partial widths were calculated using the procedure described in Sec. II A [Eq. (2), with $C^2=1$ for $^{25}\mathrm{Al}+p$]. Single-particle spectroscopic factors have been adopted either from the corresponding ^{26}Mg mirror states (see Ref. [30]) or were taken from shell-model calculations by using the Ormand-Brown interaction (Sec. V B). Values for Γ_γ were also taken from the shell model. We note that for positive parity levels the shell model reproduces both the S values measured in the $^{25}\mathrm{Mg}(d,p)^{26}\mathrm{Mg}$ transfer reaction and the experimental lifetimes of ^{26}Mg levels within a factor of 2. A summary of estimated resonance properties for ^{26}Si states near the proton threshold is presented in Table XI. The resulting stellar reaction rate contribution of narrow resonances is listed in column 2 of Table XII.

The (nonresonant) direct capture (DC) contribution into all ^{26}Si bound states was determined following the formalism described in Ref. [63]. The radial wave function for the bound final state was calculated by using a Woods-Saxon potential ($r=1.25$ fm and $a=0.65$ fm). The well depth is chosen to reproduce the binding energy of each final state. For the calculation of the initial state radial wave function we have employed hard-sphere phase shifts. The total DC cross section is given by an incoherent sum over orbital angular momenta ℓ_i and ℓ_f for all incoming and outgoing partial waves involved:

$$\sigma_{\mathrm{total}}^{\mathrm{DC}}=\sum_{\ell_i,\ell_f}C^2S(\ell_f)\,\sigma_{\mathrm{theor}}^{\mathrm{DC}}(\ell_i,\ell_f). \tag{7}$$

The spectroscopic factors for the bound ^{26}Si states were again taken either from the ^{26}Mg mirror levels or from shell-model calculations. The total DC cross section was converted into the astrophysical S factor,

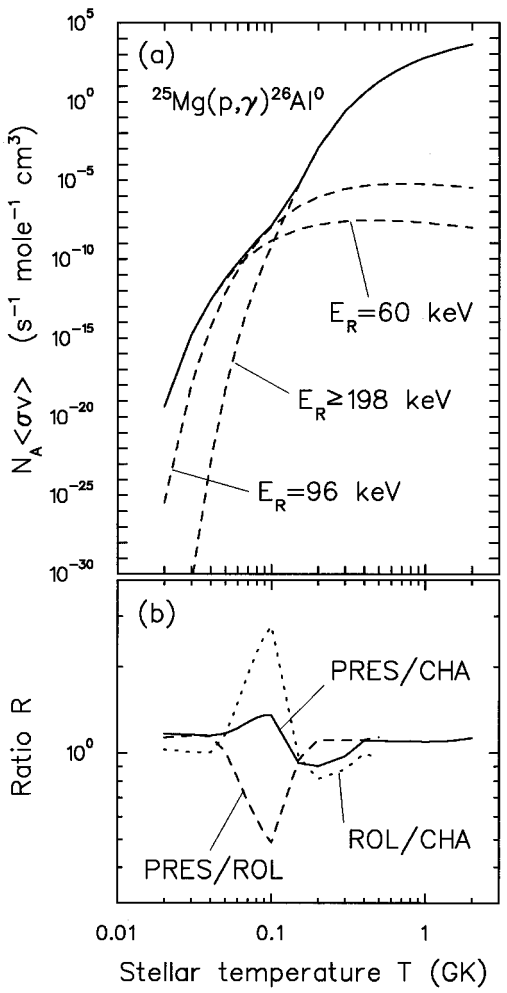

FIG. 6. (a) Total reaction rate (solid line) and individual contributions (dashed lines) for the reaction ^{25}Mg$(p,\gamma)^{26}$Al^0; (b) ratio of the present rate to the reaction rates of Champagne *et al.* [12] (solid line) and Rollefson *et al.* [13] (dashed line). The dotted line shows the ratio of rates from the previous works [12,13].

$$S(E)=\sigma(E)E\exp(2\pi\eta) \tag{8}$$

(with η denoting the Sommerfeld parameter). The S factor was found to be nearly energy independent below $E_p=1$ MeV with $S(0)=27.0$ keV b. The stellar reaction rates for the DC process calculated by using the expressions for nonresonant reaction mechanisms [60] are listed in column 3 of Table XII.

The total stellar rates for ^{25}Al$+p$, which we recommend for use in stellar network calculations, are presented in column 4 of Table XII and are displayed in Fig. 7(a) together with individual contributions. The total reaction rates are determined by the direct capture process and the resonances at $E_R=44$ and 452 keV, corresponding to the shell-model states of 1_1^+ and 3_3^+, respectively. The present reaction rates are compared in Fig. 7(b) to the previous results of Ref. [14], which are also listed in column 7 of Table XII. The latter values have been derived by using systematic nuclear trends and different analog assignments. It can be seen from Fig. 7(b) that our stellar rates deviate up to 3–4 orders of magnitude from the previous results for temperatures $T>0.01$ GK.

It should be noted that the largest uncertainties in $N_A\langle\sigma v\rangle$ result from the errors in the resonance energies (Table XI), since the quantity E_R enters exponentially in the calculation of the resonant reaction rates [Eq. (5)]. In order to estimate quantitatively the uncertainties involved we have varied the energies of single resonances within their limits presented in Table XI. The obtained resonant reaction rates, for which the energy dependence of the proton partial widths Γ_p was taken explicitly into account, were added to the DC contribution. The smallest and largest total stellar rates resulting from this procedure for different stellar temperatures T are listed in columns 5 and 6 of Table XII, respectively. It follows that the 28 keV (100 keV) error in E_R for the 44 keV (452 keV) resonance yields a maximum uncertainty in the total reaction rates of a factor 560 (750) at $T=0.015$ GK ($T=0.15$ GK).

In order to investigate qualitatively the competition between the β decay of ^{25}Al and the ^{25}Al$(p,\gamma)^{26}$Si reaction

TABLE XI. Parameters of low-energy resonances in ^{25}Al$(p,\gamma)^{26}$Si.

E_x [a] (keV)	E_R [b] (keV)	J_n^π [c]	$S_{\ell=0+2}^{\text{expt}}$ [d]	$S_{\ell=0+2}^{\text{SM}}$ [e]	Γ_p [f] (eV)	$\Gamma_\gamma^{\text{expt}}$ [d] (eV)	$\Gamma_\gamma^{\text{SM}}$ [e] (eV)	$\omega\gamma$ [g] (eV)
5562±28	44±28	1_1^+		,0.0040	1.9×10^{-21}	>0.055	0.11	4.8×10^{-22}
5940±25	422±25	4_4^+	,0.10	,0.028	3.7×10^{-2}	0.0066	0.0067	4.2×10^{-3}
5940±25	422±25	0_4^+		,0.047	1.7×10^{-2}	0.0088	0.0046	3.0×10^{-4}
5970±100	452±100	3_3^+	0.12,0.31	0.14,0.33	9.2×10^{0}	0.033	0.10	5.8×10^{-2}
6350±25	832±25	2_6^+	0.008,0.11	0.028,0.071	7.9×10^{1}	0.029	0.11	4.5×10^{-2}
6451±100	933±100	4_5^+		,0.0089	2.7×10^{0}	0.024	0.017	1.2×10^{-2}
6452±100	934±100	1_2^+		,0.049	1.5×10^{1}	>0.066	0.11	2.7×10^{-2}

[a]From Table VIII for experimentally observed levels; otherwise the results of Coulomb displacement energy calculations (Table IX), with an estimated uncertainty of ±100 keV, have been used.
[b]Calculated from column 1 using $Q_{p\gamma}=(5518\pm3)$ keV [61].
[c]Shell-model assignments adopted from Table VIII.
[d]Experimental values [30] adopted from ^{26}Mg mirror states.
[e]Shell-model results for ^{26}Si states, calculated using the Ormand-Brown interaction (see text).
[f]Proton partial widths calculated from S values in columns 4 and 5, using Eq. (2).
[g]With $\omega\gamma=(2J_R+1)\Gamma_p\Gamma_\gamma/12\Gamma$.

TABLE XII. Stellar reaction rates $N_A\langle\sigma v\rangle$ [a] for $^{25}\mathrm{Al}(p,\gamma)^{26}\mathrm{Si}$.

T (GK)	Resonances [b]	DC [c]	Total [d]	Low [e]	High [e]	[f]
0.01	5.33×10^{-36}	2.06×10^{-37}	5.53×10^{-36}	2.06×10^{-37}	5.53×10^{-36}	9.79×10^{-38}
0.015	7.16×10^{-29}	1.27×10^{-31}	7.17×10^{-29}	1.27×10^{-31}	7.17×10^{-29}	6.03×10^{-32}
0.02	2.31×10^{-25}	5.65×10^{-28}	2.31×10^{-25}	5.65×10^{-28}	2.31×10^{-25}	2.69×10^{-28}
0.03	6.24×10^{-22}	2.10×10^{-23}	6.45×10^{-22}	2.10×10^{-23}	6.29×10^{-21}	1.00×10^{-23}
0.04	2.86×10^{-20}	1.59×10^{-20}	4.45×10^{-20}	1.59×10^{-20}	4.31×10^{-18}	7.59×10^{-21}
0.05	2.62×10^{-19}	1.77×10^{-18}	2.03×10^{-18}	1.77×10^{-18}	2.02×10^{-16}	1.23×10^{-18}
0.06	1.09×10^{-18}	6.41×10^{-17}	6.52×10^{-17}	6.41×10^{-17}	2.53×10^{-15}	7.11×10^{-16}
0.07	2.93×10^{-18}	1.12×10^{-15}	1.12×10^{-15}	1.12×10^{-15}	1.54×10^{-14}	1.36×10^{-13}
0.08	5.97×10^{-18}	1.19×10^{-14}	1.19×10^{-14}	1.19×10^{-14}	6.42×10^{-14}	6.99×10^{-12}
0.09	1.02×10^{-17}	8.72×10^{-14}	8.72×10^{-14}	8.72×10^{-14}	2.26×10^{-13}	1.47×10^{-10}
0.1	3.29×10^{-17}	4.84×10^{-13}	4.84×10^{-13}	4.84×10^{-13}	9.70×10^{-13}	1.65×10^{-9}
0.15	1.90×10^{-10}	2.04×10^{-10}	3.94×10^{-10}	2.88×10^{-10}	2.16×10^{-7}	2.05×10^{-6}
0.2	6.22×10^{-7}	9.11×10^{-9}	6.31×10^{-7}	2.03×10^{-7}	1.27×10^{-4}	6.39×10^{-5}
0.3	1.83×10^{-3}	1.04×10^{-6}	1.83×10^{-3}	4.00×10^{-4}	6.31×10^{-2}	2.21×10^{-3}
0.4	8.93×10^{-2}	2.04×10^{-5}	8.93×10^{-2}	1.83×10^{-2}	1.24×10^{0}	3.35×10^{-2}
0.5	8.58×10^{-1}	1.68×10^{-4}	8.58×10^{-1}	1.91×10^{-1}	6.89×10^{0}	3.04×10^{-1}
0.6	3.69×10^{0}	8.35×10^{-4}	3.69×10^{0}	9.31×10^{-1}	2.05×10^{1}	1.55×10^{0}
0.7	1.01×10^{1}	2.98×10^{-3}	1.01×10^{1}	2.90×10^{0}	4.33×10^{1}	5.24×10^{0}
0.8	2.10×10^{1}	8.52×10^{-3}	2.10×10^{1}	6.78×10^{0}	7.40×10^{1}	1.33×10^{1}
0.9	3.65×10^{1}	2.06×10^{-2}	3.65×10^{1}	1.30×10^{1}	1.09×10^{2}	2.76×10^{1}
1.0	5.58×10^{1}	4.40×10^{-2}	5.58×10^{1}	2.18×10^{1}	1.48×10^{2}	4.95×10^{1}
1.5	1.80×10^{2}	6.31×10^{-1}	1.80×10^{2}	9.74×10^{1}	3.27×10^{2}	2.73×10^{2}

[a]Reaction rates in units of reactions $\mathrm{s}^{-1}\,\mathrm{mol}^{-1}\,\mathrm{cm}^3$.
[b]Contributions of narrow resonances (see Table XI).
[c]Contribution of direct capture process.
[d]Sum of columns 2 and 3.
[e]Lower and upper limits on total $N_A\langle\sigma v\rangle$, respectively, resulting from variation of resonance energies (see text).
[f]From Ref. [14].

(Sec. I), we present in Fig. 8 temperature and density conditions for which both processes have equal strengths (assuming a hydrogen mass fraction of $X_H=0.5$). The solid line was derived from $N_A\langle\sigma v\rangle$ listed in column 4 of Table XII, while the dashed curves result from the uncertainties in the resonance energies E_R (calculated from columns 5 and 6 of Table XII). The rectangle indicates typical temperature and density ranges ($0.146<T_{9,\mathrm{peak}}<0.325$ and $2.4\times10^3<\rho_{\mathrm{initial}}<1.4\times10^4$ g/cm^3), adopted from hydrodynamical nova simulations [64]. Our results indicate that for temperatures $T<0.18$ GK the β decay of ^{25}Al is faster than the competing (p,γ) reaction. However, for $T>0.27$ GK the $^{25}\mathrm{Al}(p,\gamma)^{26}\mathrm{Si}$ reaction dominates. Therefore, the production of $^{26}\mathrm{Al}^0$ in energetic novas is likely bypassed to a large extent (Sec. I). The uncertainties involved are still large as is apparent from Fig. 8 and better reaction rates based on improved experimental results are highly desirable. Finally we note that hydrodynamical simulations incorporating our new stellar reaction rates for $^{25}\mathrm{Mg}(p,\gamma)^{26}\mathrm{Al}$ and $^{25}\mathrm{Al}(p,\gamma)^{26}\mathrm{Si}$ are in progress [65], in order to investigate the production of ^{26}Al in novas.

VIII. CONCLUSIONS

The present work describes a consistent reanalysis of all available experimental data for the $^{25}\mathrm{Mg}(^3\mathrm{He},d)^{26}\mathrm{Al}$ reaction leading to ^{26}Al threshold states. Contrary to previous procedures we use unbound-state form factors in the DWBA analysis and calculate absolute rather than relative proton widths. From the comparison of Γ_p values from proton transfer and (p,γ) work we have shown that our method applied provides meaningful results. The proton widths deduced in the present work have been used for the calculation of new stellar rates for the $^{25}\mathrm{Mg}(p,\gamma)^{26}\mathrm{Al}$ reaction. Our reaction rates differ up to a factor of 2 compared to previous results. It is also pointed out that the stellar rates at temperatures $T=0.07$–0.15 GK which are determined by the $E_R=96$ keV resonance could be more uncertain than is generally assumed, depending on the contribution of multiple-step processes to the $^{25}\mathrm{Mg}(^3\mathrm{He},d)^{26}\mathrm{Al}$ reaction mechanism. This question could be addressed with a new measurement of the $^{25}\mathrm{Mg}(p,\gamma)^{26}\mathrm{Al}$ reaction. Adopting our estimated value (Table III) for the strength of the $E_R=96$ keV resonance and using a 1 mA proton beam on a pure Mg target yields about 130 capture γ rays per day.

Spins, parities, and isospins for ^{26}Al states below $E_x=8$ MeV have been reanalyzed using experimental results and it was found that in several cases the previous assignments were erroneous. Further, we have performed shell-model calculations for the mass $A=26$ system. Correspondences of experimental with shell-model states have been made on the basis of comparing excitation energies, $J^\pi;T$ values, γ-ray

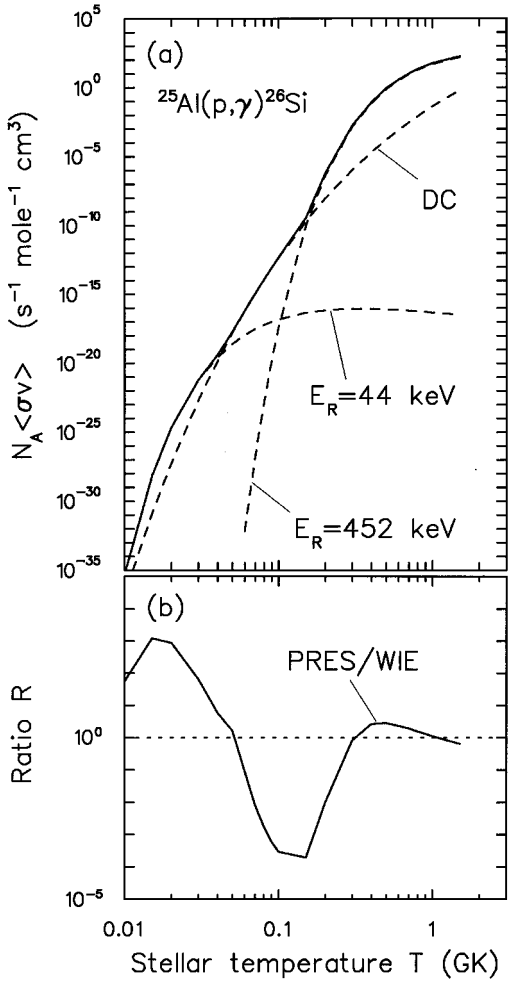

FIG. 7. (a) Total reaction rate (solid line) and individual contributions (dashed lines) for the reaction ^{25}Al$(p,\gamma)^{26}$Si; (b) ratio of the present rate to the reaction rate of Wiescher *et al.* [14].

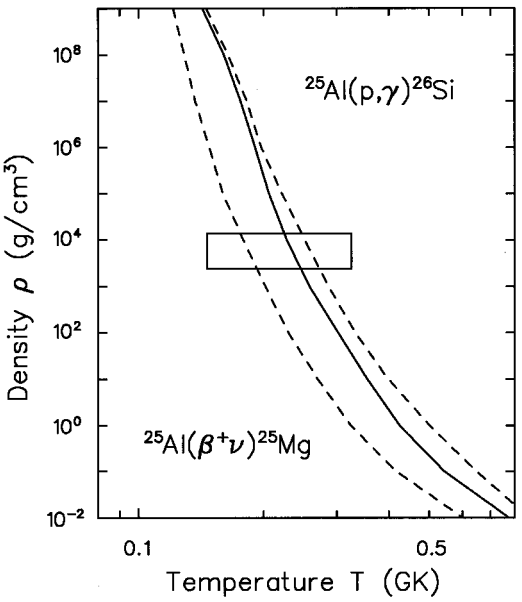

FIG. 8. Temperature-density boundary (solid line) at which the proton capture reaction on ^{25}Al and the ^{25}Al β decay are of equal strength (assuming a hydrogen mass fraction of X_H=0.5). The dashed lines result from the uncertainties in resonance energies. Temperature and density conditions typical for nova outbursts are indicated by the rectangle.

transition strengths, spectroscopic factors, and proton partial widths. Our results show that the structure of positive parity states in ^{26}Al in the excitation energy range below E_x=8 MeV is well described by the shell model.

We also have presented updated stellar rates for ^{25}Al$(p,\gamma)^{26}$Si. These are based on our new analog state assignments and results from shell-model calculations. The uncertainties involved amount up to 2–3 orders of magnitude. This reaction is of importance for the bypass of ^{26}Al^0 nucleosynthesis in nova outbursts and could be a prime target for a direct cross section measurement using radioactive nuclear beam facilities currently being proposed or constructed at several laboratories.

ACKNOWLEDGMENTS

We would like to express our appreciation to W.P. Alford, J.R. Comfort, R.J. Peterson, and M. Zeitlin for fruitful discussions. We are grateful to H. Röpke for sharing his experimental results prior to publication. One of us (C.I.) wishes to thank R.E. Azuma and J.D. King for supporting the present work. H.H. acknowledges support from the Fonds zur Förderung der wissenschaftlichen Forschung (FWF) in Austria. This work was supported in part by the Natural Sciences and Engineering Research Council of Canada and by the National Science Foundation (Grant No. PHY88-03035).

[1] W.A. Mahoney, J.C. Ling, A.S. Jacobson, and R.E. Lingenfelder, Astrophys. J. **262**, 742 (1982).
[2] G.H. Share, R.L. Kinzer, J.D. Kurfess, D.J. Forrest, E.L. Chupp, and E. Rieger, Astrophys. J. **292**, L61 (1985).
[3] C.J. MacCallum, A.F. Huters, P.D. Stang, and M. Leventhal, Astrophys. J. **317**, 877 (1987).
[4] V. Schönfelder and M. Varendorff, in *Gamma-Ray Line Astrophysics*, edited by Ph. Durouchoux and N. Prantzos, AIP Conf. Proc. No. 232 (AIP, New York, 1991), p. 101.
[5] R. Diehl *et al.*, Astron. Astrophys. **97**, 181 (1993).
[6] G. Meynet, Astrophys. J. Suppl. **92**, 441 (1994).
[7] G.J. Wasserburg, in *Protostars and Planets II*, edited by D.C. Black and M.S. Matthews (University of Arizona Press, Tucson, 1985), p. 703.
[8] N. Prantzos, in *Gamma-Ray Line Astrophysics* [4], p. 129.
[9] U. Oberlack, R. Diehl, T. Montmerle, N. Prantzos, and P. Ballmoos, Astrophys. J. Suppl. **92**, 433 (1994).
[10] R.A. Ward and W.A. Fowler, Astron. Astrophys. **238**, 266 (1980).
[11] C. Iliadis, Th. Schange, C. Rolfs, U. Schröder, E. Somorjai,

H.P. Trautvetter, K. Wolke, P.M. Endt, S.W. Kikstra, A.E. Champagne, M. Arnould, and G. Paulus, Nucl. Phys. **A512**, 509 (1990).
[12] A.E. Champagne, A.J. Howard, M.S. Smith, P.V. Magnus, and P.D. Parker, Nucl. Phys. **A505**, 384 (1989).
[13] A.A. Rollefson, V. Wijekumar, C.P. Browne, M. Wiescher, H.J. Hausman, W.Y. Kim, and P. Schmalbrock, Nucl. Phys. **A507**, 413 (1990).
[14] M. Wiescher, J. Görres, F.K. Thielemann, and H. Ritter, Astron. Astrophys. **160**, 56 (1986).
[15] P.M. Endt, P. de Wit, and C. Alderliesten, Nucl. Phys. **A459**, 61 (1986).
[16] P.M. Endt, P. de Wit, C. Alderliesten, and B.H. Wildenthal, Nucl. Phys. **A487**, 221 (1988).
[17] P.M. Endt, P. de Wit, and C. Alderliesten, Nucl. Phys. **A476**, 333 (1988).
[18] P.M. Endt and C. Rolfs, Nucl. Phys. **A467**, 261 (1987).
[19] R.R. Betts, H.T. Fortune, and D.J. Pullen, Nucl. Phys. **A299**, 412 (1978); **A312**, 524(E) (1978).
[20] G.R. Satchler, *Direct Nuclear Reactions* (Clarendon, Oxford, England, 1983).
[21] C.M. Vincent and H.T. Fortune, Phys. Rev. C **2**, 782 (1970).
[22] C.M. Vincent and H.T. Fortune, Phys. Rev. C **7**, 865 (1973).
[23] J.P. Schiffer, Nucl. Phys. **46**, 246 (1963).
[24] A.E. Champagne, A.J. Howard, and P.D. Parker, Nucl. Phys. **A402**, 179 (1983).
[25] P.D. Kunz, computer code DWUCK4 (unpublished); extended version of J.R. Comfort (unpublished).
[26] J. Vernotte, G. Berrier-Ronsin, J. Kalifa, R. Tamisier, and B.H. Wildenthal, Nucl. Phys. **A571**, 1 (1994).
[27] P.E. Hodgson, *Nuclear Reactions and Nuclear Structure* (Clarendon, Oxford, England, 1971).
[28] S.G. Cooper, R. Huby, and J.R. Mines, J. Phys. G **8**, 559 (1982).
[29] H. Nann, Nucl. Phys. **A376**, 61 (1982).
[30] P.M. Endt, Nucl. Phys. **A521**, 1 (1990).
[31] V. Landre, P. Aguer, G. Bogaert, A. Lefebvre, J.P. Thibaud, S. Fortier, J.M. Maison, and J. Vernotte, Phys. Rev. C **40**, 1972 (1989).
[32] H.T. Fortune and C.M. Vincent, Phys. Rev. **185**, 1401 (1969).
[33] C. Iliadis, J. Görres, J.G. Ross, K.W. Scheller, M. Wiescher, R.E. Azuma, G. Roters, H.P. Trautvetter, and H.C. Evans, Nucl. Phys. **A571**, 132 (1994).
[34] H. Röpke (private communication).
[35] P.M. Endt, At. Data Nucl. Data Tables **55**, 171 (1993).
[36] G. Adams, E.G. Bilpuch, G.E. Mitchell, R.O. Nelson, and C.R. Westerfeldt, J. Phys. G **10**, 1747 (1984).
[37] D.O. Boerma, A.R. Arends, P.M. Endt, W. Grüebler, V. König, P.A. Schmelzbach, and R. Risler, Nucl. Phys. **A449**, 187 (1986).
[38] V. Wijekumar, P. Schmalbrock, H.J. Hausman, T.R. Donoghue, M. Wiescher, H.R. Suiter, C.P. Browne, A.A. Rollefson, and R.W. Tarara, Nucl. Phys. **A436**, 561 (1985).
[39] R.J. Peterson, M. Yasue, M.H. Tanaka, T. Hasegawa, N. Nisimura, H. Ohnuma, H. Shimizu, K. Ieki, H. Toyokawa, M. Iwase, J. Iimura, and S.I. Hayakawa, Phys. Rev. C **38**, 1130 (1988).
[40] R.J. Peterson (private communication).
[41] M. Yasue, H. Sato, T. Hasegawa, J. Takamatsu, T. Terakawa, T. Nakagawa, K. Hatori, and R.J. Peterson, Phys. Rev. C **39**, 2159 (1989).
[42] B.A. Brown, A. Etchegoyen, and W.D.M. Rae, MSU/NSCL Report No. 524, 1985.
[43] B.A. Brown and B.H. Wildenthal, Ann. Revu. Nucl. Part. Sci. **38**, 29 (1988).
[44] M. Carchidi, B.H. Wildenthal, and B.A. Brown, Phys. Rev. C **34**, 2280 (1986).
[45] B.A. Brown and B.H. Wildenthal, Nucl. Phys. **A474**, 290 (1987).
[46] T.A. Walkiewicz, S. Raman, E.T. Jurney, J.W. Starner, and J.E. Lynn, Phys. Rev. C **45**, 1597 (1992).
[47] J. Vernotte, G. Berrier-Ronsin, S. Fortier, E. Hourani, J. Kalifa, J.M. Maison, L.H. Rosier, G. Rotbard, and B.H. Wildenthal, Phys. Rev. C **48**, 205 (1993).
[48] K.K. Seth, R. Soundranayagam, A. Saha, C.W. de Jager, H. de Vries, B.A. Brown, and B.H. Wildenthal, Phys. Rev. Lett. **74**, 642 (1995).
[49] R. Soundranayagam *et al.*, Report No. NIKHEF-K, 1995.
[50] W. Bohne, K.D. Büchs, H. Fuchs, K. Grabisch, D. Hilscher, U. Jahnke, H. Kluge, T.G. Masterson, H. Morgenstern, and B.H. Wildenthal, Nucl. Phys. **A378**, 525 (1982).
[51] W.P. Alford, P. Craig, D.A. Lind, R.S. Raymond, J. Ullman, C.D. Zafiratos, and B.H. Wildenthal, Nucl. Phys. **A457**, 317 (1986).
[52] R.A. Paddock, Phys. Rev. C **5**, 485 (1972).
[53] W.P. Alford, J.A. Cameron, E. Habib, and B.H. Wildenthal, Nucl. Phys. **A454**, 189 (1986).
[54] R.A.I. Bell, J. L'Ecuyer, R.D. Gill, B.C. Robertson, I.S. Towner, and H.J. Rose, Nucl. Phys. **A133**, 337 (1969).
[55] H. Herndl, J. Görres, M. Wiescher, B.A. Brown, and L. Van Wormer, Phys. Rev. C **52**, 1078 (1995).
[56] W.E. Ormand and B.A. Brown, Nucl. Phys. **A491**, 1 (1989).
[57] R.G. Thomas, Phys. Rev. **81**, 148 (1951).
[58] S.B. Ehrman, Phys. Rev. **81**, 412 (1951).
[59] C. Iliadis, Diplom thesis, Universität Münster, 1989.
[60] W.A. Fowler, G.R. Caughlan, and B.A. Zimmerman, Annu. Rev. Astron. Astrophys. **5**, 525 (1967).
[61] G. Audi and A.H. Wapstra, Nucl. Phys. **A565**, 66 (1993).
[62] M.R. Anderson, L.W. Mitchell, M.E. Sevior, S.R. Kennett, and D.G. Sargood, Nucl. Phys. **A373**, 326 (1982).
[63] C. Rolfs, Nucl. Phys. **A217**, 29 (1973).
[64] S. Starrfield, J.W. Truran, and W.M. Sparks, Astrophys. J. **226**, 186 (1978).
[65] S. Starrfield (private communication).
[66] R.H. Bassel, Phys. Rev. **149**, 791 (1966).
[67] C.M. Perey and F.G. Perey, At. Data Nucl. Data Tables **17**, 1 (1976).
[68] K.K. Seth, J.A. Biggerstaff, P.D. Miller, and G.R. Satchler, Phys. Rev. **164**, 1450 (1967).